Geochimica et Cosmochimica Acta, Vol. 68, No. 24, pp. 5169–5188, 2004

0016-7037/04 $30.00 + .00

doi:10.1016/j.gca.2004.05.041

Shear viscosities of $CaO-Al_2O_3-SiO_2$ and $MgO-Al_2O_3-SiO_2$ liquids: Implications for the structural role of aluminium and the degree of polymerisation of synthetic and natural aluminosilicate melts

MICHAEL J. TOPLIS [1,*†] and DONALD B. DINGWELL[2]

[1]Center de Recherches Pétrographiques et Géochimiques. 15, rue Notre-Dame des Pauvres, F-54501, Vandoeuvre, France
[2]Department of Earth and Environmental Sciences, University of Munich, Theresienstr.41/III, D-80333 Munich, Germany

(*Received January* 15, 2004; *accepted in revised form* May 14, 2004)

Abstract—The shear viscosity of 66 liquids in the systems $CaO-Al_2O_3-SiO_2$ (CAS) and $MgO-Al_2O_3-SiO_2$ (MAS) have been measured in the ranges $1–10^4$ Pa s and $10^8–10^{12}$ Pa s. Liquids belong to series, nominally at 50, 67, and 75 mol.% SiO_2, with atomic $M^{2+}/(M^{2+}+2Al)$ typically in the range 0.60 to 0.40 for each isopleth. In the system CAS at 1600°C, viscosity passes through a maximum at all silica contents. The maxima are clearly centered in the peraluminous field, but the exact composition at which viscosity is a maximum is poorly defined. Similar features are observed at 900°C. In contrast, data for the system MAS at 1600°C show that viscosity decreases with decreasing Mg/(Mg + 2Al) at all silica contents, but that a maximum in viscosity must occur in the field where Mg/2Al >1. On the other hand, the viscosity at 850°C increases with decreasing Mg/(Mg + 2Al) and shows no sign of reaching a maximum, even for the most peraluminous composition studied. The data from both systems at 1600°C have been analysed assuming that shear viscosity is proportional to average bond strength and considering the equilibrium:

$$Al^{[4]}\text{-}(Mg, Ca)_{0.5} \Leftrightarrow (Mg,Ca)_{0.5}\text{-NBO} + Al_{XS}$$

where $Al^{[4]}$-$(Mg,Ca)_{0.5}$ represents a charge-balanced tetrahedrally coordinated Al; $(Mg, Ca)_{0.5}$–NBO represents a nonbridging oxygen (NBO) associated with Ca or Mg, and Al_{XS} represents any structural role of Al that does not require a charge-balancing cation. The viscosity data were fitted using two adjustable variables: i) the equilibrium constant of the above reaction, and ii) the relative bond strength of Al_{XS}. The values of these parameters in the system CAS suggest that Al_{XS} remains in tetrahedral coordination, its charge deficit being satisfied by association with a three-coordinate oxygen in a structure called a tricluster. In contrast, fits to the MAS data at 1600°C infer the presence of high-coordinate Al. These interpretations are found to be consistent with independent spectroscopic and theoretical data. Furthermore, the fitted value of the equilibrium constant in the system MAS is close to zero, implying that Al has no thermodynamic preference to be charge-balanced by Mg. In light of these results, it is shown that values of the ratio 'NBO/T' (the ratio of NBO to tetrahedrally coordinated network formers) will not be a true reflection of the polymerisation state of the liquid if it is assumed that all Al is charge-balanced by metal cations. This will be important to take into account when considering the compositional dependence of physical and thermodynamic parameters and may have direct relevance to certain liquids produced during partial melting of the mantle.

1. INTRODUCTION

Based upon comparison of the spectroscopic features of aluminosilicate minerals and their corresponding glasses (Taylor and Brown, 1979a,b), it is generally accepted that Al^{3+} has a strong preference for tetrahedral coordination in amorphous aluminosilicates, its charge deficit being compensated by association with a low field strength cation, M^{n+}, such as Na^+, Ca^{2+} (see also Mysen, 1988). A polymerising effect of the addition of Al and an association of Al with low-field strength cations is further supported by the variations of physical and thermodynamic properties in simple aluminosilicate systems (Riebling, 1966; Roy and Navrotsky, 1984). Most considerations of silicate melts therefore assume that aluminium occurs in tetrahedral coordination associated with charge-balancing cations in all liquids with $(M^{n+}/nAl) \geq 1$, the limiting case $M^{n+}/nAl = 1$ representing the stoichiometric limit at which all metal cations are associated with Al. In this case the network is fully polymerized as in crystalline tectosilicates, that is to say, the liquid contains no cations in network-modifying roles and no nonbridging oxygens (NBO).

However, in recent years, it has become increasingly clear that the structure of melts in which the nominal number of NBO approaches zero is more complex than the simple model presented above. For example, a ^{17}O nuclear magnetic resonance (NMR) study of anorthite glass ($CaAl_2Si_2O_8$) shows the presence of ~5% of nonbridging oxygens where none would be predicted (Stebbins and Xu, 1997). Similarly, in the system $MgO-Al_2O_3-SiO_2$, ^{27}Al NMR has demonstrated the existence of high-coordinate Al in glasses with Mg/2Al = 1 (McMillan and Kirkpatrick, 1992; Toplis et al., 2000), again where no such species would be predicted by models based upon stoichiometry alone. Furthermore, indirect evidence that nonbridging

* Author to whom correspondence should be addressed (toplis@pontos.cst.cnes.fr).
† *Present address:* DTP-UMR5562, Observatoire Midi-Pyrénées, 14, Ave. Edouard Belin, 31400 Toulouse, France

oxygens occur in tectosilicate liquids in the system Na_2O-Al_2O_3-SiO_2 has been provided by viscosity measurements which show that at constant temperature a maximum in viscosity occurs in the vicinity of the metaluminous join but that this maximum is clearly displaced to the peraluminous side of the join (Toplis et al., 1997). Molecular dynamics simulations also suggest that NBO can exist in tectosilicate liquids (Scamehorn and Angell, 1991; Nevins and Spera, 1998; Morgan and Spera, 2001).

Assessing the number of NBO in silicate liquids may be of considerable importance given that many physical and thermodynamic properties, including viscosity (Behrens and Schulze, 2003), mineral–liquid element partitioning (Kohn and Schofield, 1994; Toplis and Corgne, 2002; Kushiro and Walter, 1998), redox equilibria (Mysen et al., 1984), thermodynamic activities (Beckett, 2002), noble gas solubilities (Shibata et al., 1998), and diffusivity of oxygen (Tinker et al., 2003) have all been found to show continuous variations as a function of the parameter 'NBO/T', the ratio of NBO to tetrahedrally coordinated network formers (Mysen, 1988).

Thus, it is timely to consider in detail the validity of the idea that all Al is associated with a charge-balancing cation in liquids with $(M^{n+}/n\mathrm{Al}) \geq 1$, an assumption central to the calculation of NBO/T from stoichiometry alone (e.g., equation of Mysen et al., 1984). In this work, we extend the study of Toplis et al. (1997) to calcium and magnesium bearing systems with the aim of quantifying to what extent some aluminium may not be associated with metal cations in liquids with $(M^{n+}/n\mathrm{Al}) \geq 1$, to determine the structural role of such aluminium and to assess whether this latter is a function or not of the metal cations present in the liquid. We will end by considering the implications of these results for natural silicate liquids.

2. EXPERIMENTAL METHODS

2.1. Sample Preparation and Analysis

Almost 70 compositions close to the charge-balanced joins in the systems CaO-Al_2O_3-SiO_2 (CAS) and MgO-Al_2O_3-SiO_2 (MAS) have been studied. Glasses belong to series, nominally at 50, 67, and 75 mol.% SiO_2, with atomic $(M^{2+}/(M^{2+}+2\mathrm{Al}))$ typically in the range, 0.60 to 0.40 for each isopleth. To avoid random variations in SiO_2 content in a given compositional series, a peraluminous and peralkaline endmember composition were first prepared along each silica isopleth. ~300 g of each endmember glass were made from mixtures of reagent grade SiO_2, Al_2O_3, MgO, and $CaCO_3$, melted at 1600°C in thin-walled 75-cc Pt crucibles. After at least 1 h, liquids were poured onto a steel plate, cooled to a glass, then coarsely crushed and remelted for another hour. The glasses produced by this second melting were finely crushed in an automated Retsch agate mortar. Intermediate compositions were made from weighed mixtures of the endmember glass powders which were mechanically mixed before melting and then fully homogenised during the initial stages of the concentric cylinder viscosity measurements described below. To provide a closer spacing of composition, a second set of endmember glasses (distinguished by the suffix 'b' in Table 1) was synthesised for the compositional series CAS at 75 and 67 mol.% SiO_2.

Chips of glass were recovered after homogenisation during high-temperature viscosity measurements, mounted in epoxy, then polished. Sample compositions (shown in Table 1) were subsequently determined using an SX50 electron microprobe running at 15 kV, 10 nA and a defocused beam diameter of 20 microns.

2.2. 'High-Temperature' Viscosity Measurements

Viscosities were initially determined in the range 1 to 10^4 Pa s using the concentric cylinder method. The viscometer head is a Brookfield DV-III, with a full-scale torque of 7.20×10^{-2} N-m. The spindle and crucible are made from $Pt_{80}Rh_{20}$, and the spindle geometry is identical to that described by Dingwell and Virgo (1987). This apparatus, its mode of operation, and modifications to the software and hardware are described in Dingwell (1989). Rotation rates between 0.1 and 100 rpm were used with higher rotation rates used at higher temperature. Measurements were begun at the highest temperature, and temperature reduced, generally in steps of 50K, until crystallization occurred or an instrumental limit was reached. At the end of the lowest temperature measurement, the highest temperature condition was reoccupied. If the final reading was not within ±0.5% of the initial reading, the entire measurement process was repeated. Once cooled to room temperature, cylinders of glass were cored from the crucible, then prepared for low-temperature viscosity measurements.

Viscosities were calculated by calibrating the crucible, spindle, and head combination using the German standard glass DGG-1, with a stated accuracy of ±5%. However, the precision of measurements is significantly better than this. Indeed, during the course of this study replicate measurements show that when the centering and immersion of the spindle are identical, a precision of <0.5% (0.002 $\log_{10}$ units) is possible. Given that changing samples may result in small variations in these geometrical parameters, five samples in the series MAS67 were run twice to estimate the real precision when measuring different compositions. In light of these results (Table 2), our stated precision is ±1% (±0.005 $\log_{10}$ units).

2.3. 'Low-Temperature' Viscosity Measurements

Two different techniques were used to measure viscosity in the range 10^8 to 10^{12} Pa s. The first is micropenetration (employed for glasses in the series CAS50), which involves determining the rate at which a hemispherical Ir indenter (diameter, 2 mm) moves into the melt surface under a fixed load of 1.2 N. These measurements were performed using a BÄHR DIL 802V vertical push-rod dilatometer, equipped with a silica sample holder under an Ar gas flow. Viscosities determined on lead-silicate SRM-711 have been reproduced within ±0.06 log units. Further details of this apparatus and its operating mode are described by Hess et al. (1995).

The second technique (employed for the series MAS50) uses the uniaxial compression device described by Neuville and Richet (1991). This technique involves measuring the deformation rate of cylinders, typically 5 mm in diameter and 10 mm in height, in air under uniaxial stresses in the range 1–200N, higher viscosities being measured at higher stresses. For a given stress, measurements of sample height as a function of time may be used to calculate the viscosity, as described by Neuville and Richet (1991). At each temperature at least three different stresses were applied to check the Newtonian nature of the viscosity. Measurements on NBS standard glass 710 show discrepancies of less than 0.04 log units with recommended values. The two techniques employed provide consistent data as illustrated in Figure 1 for a liquid of anorthite composition ($CaAl_2Si_2O_8$).

3. RESULTS

3.1. Variations of Viscosity as a Function of Temperature

Shear viscosity measurements made in the low and high viscosity range are summarised in Tables 2 and 3 respectively. When the concentric cylinder measurements are considered as a function of temperature, data for each composition may be described by the equation:

$$\log \eta = A + B/T \quad (1)$$

where η is viscosity in Pa s, T is absolute temperature, and A and B are fit parameters whose values are shown in Table 4.

Table 1. Chemical compositions of the studied glasses.

	wt.%SiO_2	wt.%Al_2O_3	wt.%CaO	Total	mol.% SiO_2	molar Ca*[a]
CAS75a:61	70.49(56)[b]	15.77(8)[b]	13.32(9)[b]	99.58	74.95	60.55
CAS75a:58	70.06(19)	16.35(9)	12.29(5)	98.70	75.44	57.76
CAS75a:56	69.86(37)	17.54(9)	12.32(15)	99.73	74.80	56.09
CAS75a:54	68.42(118)	18.90(72)	12.17(35)	99.49	73.89	53.94
CAS75a:53	69.52(28)	18.61(10)	11.50(10)	99.63	74.91	52.90
CAS75a:50	69.36(73)	18.75(51)	10.32(30)	98.43	75.83	50.02
CAS75a:49	68.05(28)	19.81(9)	10.28(9)	98.13	75.00	48.54
CAS75a:47	69.01(44)	20.33(14)	9.87(8)	99.20	75.37	46.87
CAS75a:45	68.67(52)	21.28(7)	9.72(10)	99.68	74.95	45.36
CAS75a:44	70.05(52)	20.86(49)	9.02(14)	99.92	76.14	44.01
CAS75a:41	67.82(54)	22.69(10)	8.64(11)	99.15	74.98	40.90
CAS75b:55	69.18(24)	17.93(45)	11.87(11)	98.98	74.82	54.64
CAS75b:53	68.93(56)	18.91(27)	11.65(19)	99.50	74.47	52.83
CAS75b:52	68.27(90)	19.21(63)	11.47(40)	98.96	74.30	52.05
CAS75b:51	67.24(37)	20.19(30)	11.52(18)	98.95	73.50	50.93
CAS75b:50.5	68.35(56)	19.89(43)	11.11(15)	99.35	74.31	50.40
CAS75b:50	67.98(23)	20.13(19)	10.98(27)	99.09	74.21	49.79
CAS75b:49	68.50(48)	20.25(27)	10.60(21)	99.35	74.63	48.75
CAS75b:47.5	68.00(38)	20.83(24)	10.35(23)	99.18	74.43	47.46
CAS75b:46	68.32(39)	21.31(30)	9.97(25)	99.60	74.61	45.98
CAS75b:43.5	68.10(31)	22.19(50)	9.38(16)	99.67	74.65	43.45
CAS67a:57	61.09(32)	22.59(11)	16.20(11)	99.88	66.58	56.58
CAS67a:54	60.81(26)	23.77(15)	15.08(8)	99.66	66.84	53.56
CAS67a:52	59.69(44)	25.00(27)	14.93(15)	99.62	66.01	52.05
CAS67a:50	60.10(34)	25.67(13)	13.91(13)	99.68	66.68	49.62
CAS67a:47	59.88(32)	26.79(18)	13.27(3)	99.95	66.62	47.39
CAS67a:46	59.74(17)	27.77(9)	12.76(11)	100.27	66.54	45.53
CAS67a:41	58.96(28)	29.42(9)	11.42(6)	99.79	66.60	41.37
CAS67b:55	60.80(22)	23.57(10)	15.43(8)	99.79	66.65	54.33
CAS67b:53	60.94(27)	23.87(15)	14.83(8)	99.65	67.04	53.04
CAS67b:52	60.00(12)	24.72(9)	14.73(13)	99.46	66.41	52.00
CAS67b:51	60.19(20)	24.85(5)	14.26(16)	99.29	66.80	51.06
CAS67b:50	59.74(40)	24.96(19)	13.90(10)	98.60	66.86	50.31
CAS67b:49	60.06(14)	25.81(10)	13.66(9)	99.53	66.80	49.04
CAS67b:48	60.50(18)	26.20(10)	13.25(9)	99.96	67.12	47.91
CAS50:61	44.66(30)	29.28(7)	25.61(6)	99.55	49.98	61.40
CAS50:57	44.31(28)	31.89(16)	23.33(9)	99.53	50.29	57.08
CAS50:54	44.06(15)	33.93(13)	21.75(11)	99.74	50.43	53.82
CAS50:52	43.40(32)	35.16(11)	20.87(13)	99.42	50.18	51.91
CAS50:50	42.99(24)	36.09(16)	19.90(15)	98.98	50.23	50.07
CAS50:48	42.59(24)	37.26(15)	18.90(7)	98.75	50.23	47.98
CAS50:46	43.27(27)	38.20(10)	18.13(8)	99.60	50.78	46.31
CAS50:45	43.10(23)	38.93(19)	17.24(12)	99.27	51.00	44.60
CAS50:44	43.78(31)	38.95(6)	16.83(12)	99.56	51.65	43.99
MAS75:58	73.30(35)[b]	17.18(35)[b]	9.30(17)[b]	99.78	75.34	57.79
MAS75:57	72.89(28)	17.43(20)	9.16(7)	99.48	75.29	57.06
MAS75:55	72.46(32)	17.98(13)	8.73(18)	99.17	75.43	55.10
MAS75:53	72.15(47)	19.24(40)	8.46(10)	99.86	75.08	52.66
MAS75:51	71.58(31)	19.74(37)	8.04(15)	99.36	75.19	50.73
MAS75:49	71.22(37)	20.40(27)	7.62(13)	99.25	75.28	48.58
MAS75:46	69.46(113)	22.60(112)	7.61(40)	99.66	73.80	45.98
MAS67:58	64.03(46)	22.83(24)	12.42(17)	99.29	66.70	57.92
MAS67:56	63.26(82)	24.15(83)	12.18(39)	99.59	66.15	56.05
MAS67:53	62.28(25)	26.11(46)	11.43(26)	99.82	65.77	52.55
MAS67:50	62.46(59)	26.59(44)	10.36(17)	99.41	66.76	49.63
MAS67:48	61.98(42)	27.52(49)	10.03(23)	99.53	66.54	47.96
MAS67:46	62.24(58)	28.04(56)	9.51(18)	99.80	66.97	46.17
MAS67:44	62.15(63)	28.43(48)	8.69(10)	99.27	67.67	43.60
MAS50:55	49.28(35)	33.75(47)	16.49(21)	99.53	52.56	55.28
MAS50:54	48.78(61)	34.90(45)	16.21(25)	99.89	52.17	54.02
MAS50:52	48.43(33)	36.04(28)	15.72(35)	100.19	52.02	52.45
MAS50:50	47.59(46)	36.83(49)	14.85(13)	99.27	52.05	50.49
MAS50:49	47.19(44)	38.33(57)	14.50(25)	100.03	51.64	48.91
MAS50:47	46.46(19)	39.55(39)	13.84(20)	99.85	51.40	46.94
MAS50:45	45.92(28)	40.63(56)	13.31(27)	99.86	51.19	45.32
MAS50:44	45.17(60)	41.70(38)	12.73(26)	99.60	50.92	43.56

[a] Ca* represents the molar ratio [CaO/(CaO + Al_2O_3)].
[b] Numbers in parentheses correspond to uncertainty in terms of the least units cited.
[c] Mg* represents the molar ratio [MgO/(MgO + Al_2O_3)].

Table 2. Measured viscosities (expressed as $\log_{10}\eta$ in Pas) for each composition.

CAS75a:	61	58	56	54	53	50	49	47	45	44	41
T (°C)	$\log_{10}\eta$ (Pa s)										
1600	1.898	1.935	1.970	2.001	2.012	2.049	2.041	2.042	2.048	2.027	2.011
1550	2.139	2.188	2.230	2.264	2.278	2.315	2.311	2.314	2.322	2.301	2.288
1500	2.400	2.464	2.511	2.550	2.571	2.609	2.609	2.611	2.622	2.603	2.590
1450	2.690	2.764	2.818	2.860	2.885	2.928	2.932	2.935	2.948	2.928	2.918
1400	3.006	3.092	3.153	3.200	3.232	3.279	3.288	3.290	3.307	3.288	
1350	3.340	3.438	3.508	3.560	3.599	3.653	3.666	3.669	3.690	3.672	
1300		3.844	3.924	3.986	4.032	4.093	4.111	4.116	4.141	4.124	

CAS75b:	55	53	52	51	50.5	50	49	47.5	46	43.5
T (°C)	$\log_{10}\eta$ (Pa s)									
1650	1.762	1.782	1.792	1.792	1.808	1.793	1.793			
1600	1.993	2.018	2.029	2.035	2.046	2.037	2.039	2.037	2.044	2.040
1550	2.251	2.280	2.293	2.304	2.314	2.302	2.309	2.309	2.319	2.315
1500	2.534	2.567	2.582	2.587	2.607	2.597	2.604	2.606	2.618	2.615
1450	2.841	2.880	2.897	2.906	2.927	2.917	2.926	2.931	2.945	2.945
1400	3.176	3.222	3.240	3.252	3.277	3.269	3.282	3.287	3.305	3.306

CAS67a:	57	54	52	50	47	46	41
T (°C)	$\log_{10}\eta$ (Pa s)						
1600	1.297	1.324	1.340	1.339	1.346	1.341	1.315
1550	1.538	1.573	1.592	1.594	1.604	1.599	1.575
1500	1.803	1.846	1.870	1.874	1.888	1.884	1.862
1450	2.096	2.148	2.177	2.186	2.203	2.201	
1400	2.424	2.487	2.521	2.535	2.554	2.555	
1350	2.790	2.866	2.905	2.925	2.954		
1300	3.201	3.294	3.340	3.366	3.396		

CAS67b:	55	53	52	51	50	49	48
T (°C)	$\log_{10}\eta$ (Pa s)						
1600	1.317	1.343	1.341		1.353		1.347
1550	1.562	1.590	1.590	1.593	1.604	1.597	1.600
1500	1.832	1.862	1.865	1.868	1.882	1.877	1.880
1450	2.130	2.164	2.169	2.175	2.191	2.188	2.192
1400	2.465	2.504	2.512	2.519	2.538	2.537	2.542
1350	2.841	2.885	2.896	2.906	2.928	2.929	2.935
1300	3.130	3.318					

CAS50:	61	57	54	52	50	48	46	45	44
T (°C)	$\log_{10}\eta$ (Pa s)								
1680									0.096
1660									0.165
1650								0.202	0.203
1640									0.239
1625								0.296	0.276
1620									0.314
1600	0.263	0.332	0.367	0.377	0.392	0.395	0.403	0.397	0.395
1550	0.450	0.535	0.576	0.589	0.605	0.610	0.619		
1500	0.665	0.760	0.806	0.823	0.843	0.849			
1450	0.902	1.014	1.066	1.087	1.108	1.117			
1400	1.172	1.300	1.360	1.386	1.412				
1350	1.484	1.634	1.704	1.735					
1300		2.018	2.105						

Viscosity at fixed temperature is a function of SiO_2 content, being greatest at higher silica content, as illustrated in Figure 2. This is true for both CAS and MAS liquids, although it may be noted that at the same temperature and silica content magnesium silicates have lower viscosity than corresponding calcium-bearing compositions. At constant silica content, viscosity is not a strong function of M/(M + 2Al), in particular for liquids in the system MAS (Fig. 2). However, systematic variations of viscosity do occur at constant temperature and silica content, and these will be presented and discussed below.

Table 2. (Continued)

MAS75: T (°C)	58	57	55	53	51	49	46
	$\log_{10}\eta$ (Pa s)						
1640	1.723	1.720		1.697	1.682	1.656	1.636
1620	1.813	1.813	1.821	1.791	1.777	1.750	1.729
1615	1.838						
1600	1.912	1.911	1.919	1.889	1.874	1.848	1.827
1575			2.043	2.015	2.001	1.974	1.955
1550	2.170		2.178	2.150	2.135	2.108	2.089
1525			2.314	2.288	2.274	2.248	2.230
1500	2.451		2.462	2.435	2.418	2.393	2.375
1475			2.611				

MAS67a T (°C)	53	50	48	46	44
	$\log_{10}\eta$ (Pa s)				
1600	1.161	1.156	1.147	1.141	1.124
1550	1.398	1.393	1.386	1.381	1.364
1500	1.664	1.661	1.655	1.651	1.637
1450	1.955	1.953	1.950		
1400	2.282	2.284			
1350	2.647				

MAS67b: T (°C)	58a	58b	56	53	50	48	46
	$\log_{10}\eta$ (Pa s)						
1600	1.181	1.174	1.183	1.170	1.154	1.157	1.143
1550	1.405		1.413	1.398	1.384	1.391	1.376
1500	1.662	1.658	1.672	1.657	1.646	1.655	1.643
1450	1.942		1.955	1.941	1.933	1.945	
1400	2.257	2.254	2.272	2.260	2.255		

MAS50: T (°C)	55a	55b	54	52	50	49	47	45	44
	$\log_{10}\eta$ (Pa s)								
1620									0.127
1600	0.212	0.210	0.215	0.211	0.212	0.212	0.208	0.202	0.200
1575						0.309	0.304		
1550	0.405	0.404	0.403	0.407	0.409	0.410			
1525					0.515				
1500	0.619	0.617	0.623	0.624					
1475			0.740	0.742					
1450	0.857	0.854	0.862						

The data collected in the range 10^8 to 10^{12} Pa s may also be satisfactorily described by Eqn. 1 (Fig. 3) with relevant values of the fit parameters shown in Table 4. In this respect, it is of note that for a given composition, the temperature dependence of viscosity at low temperature is considerably greater than that at high temperature (Table 4). In other words, over large temperature ranges, viscosity is non-Arrhenian, a common feature of silicate liquids (Richet and Bottinga, 1995). Where viscosity has been measured at both high and low temperature, the combined data sets have been fitted to the Tamann-Vogel-Fulcher (TVF) equation:

$$\log \eta = A_{TVF} + B_{TVF}/(T - C_{TVF}) \quad (2)$$

for which the values of parameters A_{TVF}, B_{TVF}, and C_{TVF} are shown in Table 5.

3.2. Isothermal Variations of Viscosity in the System CaO-Al_2O_3-SiO_2

In the system CaO-Al_2O_3-SiO_2, the variation of viscosity across the metaluminous join at constant temperature is qualitatively similar for all three isopleths of silica content. In all cases, viscosity passes through a maximum in the studied range of composition, but this maximum is broad and the position of the maximum ill-defined (Fig. 4). This behaviour is consistent with measurements at 1800°C in the same system by Rossin et al. (1964), illustrated in Bottinga and Weill (1972). In detail our measurements show that for all compositions with Ca/2Al > 1, viscosity increases as the ratio Ca/(Ca + 2Al) decreases. At 75 mol.% SiO_2 and 1600°C, the increase in viscosity with decreasing Ca/(Ca + 2Al) is interrupted more or less at the metaluminous join. For values of Ca/(Ca + 2Al) in the range 0.5 to 0.45 there is some suggestion that viscosity may show complex behav-

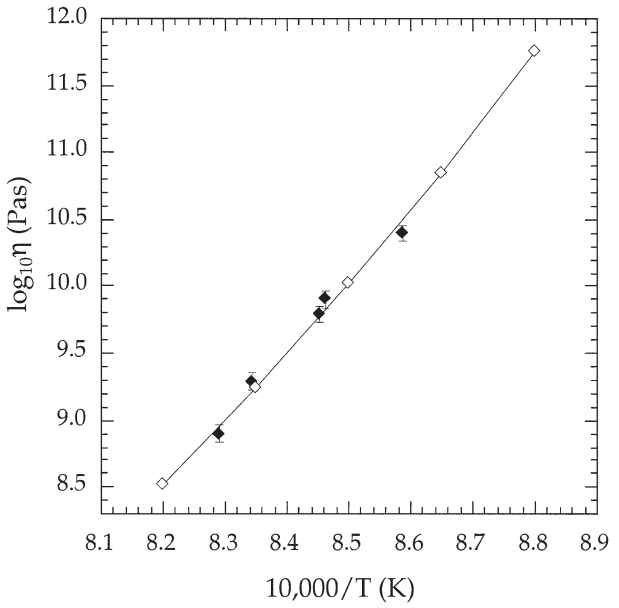

Fig. 1. Viscosity data for anorthite liquid (CAS50:50) as a function of inverse temperature. Open diamonds are measurements of Neuville (1992) made under uniaxial compression. Black diamonds are data of this study measured using the micropenetration technique.

iour with a local minimum (Fig. 4a) but these variations are of the same order of magnitude as our experimental precision. For Ca/(Ca + 2Al) < 0.45, viscosity clearly trends to lower values (Fig. 4a). For liquids with 67 mol.% SiO_2 at 1550°C, the same general features are apparent (Fig. 4b), of particular note being the approximately constant values of viscosity for Ca/(Ca + 2Al) in the range 0.5 to 0.45. Along the 50 mol.% SiO_2 join at 1600°C the compositional dependence of viscosity appears to be somewhat simpler, with a maximum in viscosity at a value of Ca/(Ca + 2Al) close to 0.46 (Fig. 4c), although we note that the number of compositions studied along this join is less than at higher silica content, thus definition of the variation of viscosity is less detailed. We also note that agreement with literature data along this join (Urbain et al., 1982; Tauber and Arndt, 1987) is excellent.

For the joins at 75 and 67 mol.% SiO_2, the studied range of temperature is limited, but at 1400°C one observes that the variation of viscosity is somewhat smoother than at 1600°C, with a more clearly defined maximum centered in the peraluminous field, at a value of Ca/(Ca + 2Al) of ~0.45 (Fig. 4d,e). At 50 mol.% SiO_2 where we have measurements close to the glass transition, data have been interpolated, using the fits to Eqn. 1, to a common temperature of 900°C (Fig. 4f). This shows that with decreasing Ca/(Ca + 2Al) viscosity increases steadily until Ca/(Ca + 2Al) = 0.48 after which viscosity is constant within the uncertainties of the measurements, behaviour which is thus similar to that observed at 1600°C (Fig. 4c).

In summary, in the system CAS, viscosity clearly passes through a maximum in the vicinity of the metaluminous join, but this maximum, although ill-defined, occurs to the peraluminous side of charge-balanced join. The temperature dependence is relatively weak, at least along the 50 mol.% SiO_2 isopleth where data are available over a wide range of temperature.

3.3. Isothermal Variations of Viscosity in the System $MgO-Al_2O_3-SiO_2$

In contrast to the calcium-bearing system described above, data for the system $MgO-Al_2O_3-SiO_2$ at 1600°C show that along all three isopleths of silica viscosity decreases with decreasing Mg/(Mg + 2Al), even when Mg/2Al > 1, this decrease being most pronounced at higher silica content (Fig. 5). Along the 50 mol.% SiO_2 isopleth, comparison of our data with those from the literature shows excellent agreement with the data of Riebling (1964) at the metaluminous join (e.g., Fig. 5c) and also demonstrates that viscosity passes through a maximum when Mg/(Mg + 2Al) has a value of ~0.55 (Urbain et al., 1982; Riebling, 1964; see also Fig. 5). Our data also suggest flattening of viscosity at values of Mg/(Mg + 2Al) in the range 0.55 to 0.6 at both 67 and 75 mol.% SiO_2, providing evidence that a maximum in viscosity exists at these silica contents too.

At temperatures close to the glass transition along the join at 50 mol.% SiO_2, measurements have been interpolated and the viscosity at 850°C calculated. This shows that at 850°C the variation of viscosity as a function of composition contrasts strongly with that observed at 1600°C, showing a pronounced and continuous *increase* across the whole range of studied Mg/(Mg + 2Al) with no sign of approaching a maximum, even at the most peraluminous composition studied (Fig. 5d).

3.4. Activation Energies

In addition to considering the variation of viscosity as a function of composition, it is also of interest to consider the variation of activation energy to viscous flow, a parameter directly proportional to the B term of Eqn. 1 (Activation energy = 2.303*R*B where R is the gas constant). As an example, values at 75 mol.% SiO_2 in the system CAS are illustrated in Figure 6, where it may be seen that there would appear to be an inconsistency between the values determined for compositions in series a and b. There would also appear to be a drop in activation energy for the most peraluminous composition (Fig. 6). However, measurements for different compositions were not made over identical temperature ranges; thus, to provide a more rigorous comparison, activation energies have also been calculated using only data in the temperature range 1600 to 1450 °C (shown in Table 4). When these latter values are used, it is found that the two different series of CAS75 glasses give perfectly consistent values of activation energy and that the combined data set indicates a continuous increase of activation energy with decreasing values of Ca/(Ca + 2Al), as illustrated in Figure 7a. However, the increase in activation energy is not a linear function of Ca/(Ca + 2Al), but asymptotically approaches a constant value of ~375 kJ/mol in the peraluminous field (Fig. 7a). When the data at 67 and 50 mol.% SiO_2 are

Table 3. Viscosities measured at low temperature.

CAS50:57		CAS50:54		CAS50:52		CAS50:50	
T (°C)	$\log_{10}\eta$ (Pa s)	T (°C)	$\log_{10}\eta$ (Pa s)	T (°C)	$\log_{10}\eta$ (Pa s)	T (°C)	$\log_{10}\eta$ (Pa s)
933.4	8.37	937.7	8.72	937.1	8.90	932.9	8.90
907.9	9.25	910.3	9.57	927.3	8.79	925.5	9.29
888.6	10.06	906.9	9.45	912.6	9.62	909.9	9.79
869.2	10.43	894.3	9.93	909.4	9.71	908.7	9.90
852.6	11.05	885.5	10.27	892.1	10.19	891.5	10.40
		874.1	10.71	889.4	10.50		
		866.5	11.05	866.5	11.05		
		856.4	11.21				
CAS50:48		CAS50:46		CAS50:45		CAS67:50	
T (°C)	$\log_{10}\eta$ (Pa s)	T (°C)	$\log_{10}\eta$ (Pa s)	T (°C)	$\log_{10}\eta$ (Pa s)	T (°C)	$\log_{10}\eta$ (Pa s)
940.6	8.85	938.3	9.03	940.5	9.06	958.8	8.88
923.9	9.49	921.8	9.44	912.6	9.85	939.2	9.34
913.6	9.74	910.0	10.00	907.2	9.84	909.6	10.22
912.1	10.04	903.5	10.11	892.2	10.68	865.1	11.37
891.6	10.69	891.1	10.70	874.9	11.20		
875.0	11.27	884.6	10.91				
		874.0	11.15				
MAS50:55		MAS50:52		MAS50:50		MAS50:49	
T (°C)	$\log_{10}\eta$ (Pa s)	T (°C)	$\log_{10}\eta$ (Pa s)	T (°C)	$\log_{10}\eta$ (Pa s)	T (°C)	$\log_{10}\eta$ (Pa s)
826.3	10.98	873.1	9.50	873.6	9.57	863.3	9.97
841.8	10.39	862.7	9.83	862.9	9.91	847.4	10.55
852.1	10.02	847.1	10.41	847.5	10.48	832.0	11.15
862.4	9.68	836.3	10.78	837.2	10.87	821.3	11.55
		826.3	11.18	826.5	11.28		
MAS50:47		MAS50:45		MAS50:44			
T (°C)	$\log_{10}\eta$ (Pa s)	T (°C)	$\log_{10}\eta$ (Pa s)	T (°C)	$\log_{10}\eta$ (Pa s)		
868.2	9.87	872.4	9.79	873.0	9.84		
852.5	10.44	856.8	10.35	857.7	10.39		
836.9	11.04	841.2	10.95	842.0	10.99		
820.8	11.70	825.7	11.57	826.1	11.64		

considered (using data over a fixed temperature range for each compositional series as detailed in Table 4), the form of the variation of activation energy as a function of Ca/(Ca + 2Al) is identical to that at 75 mol.% SiO_2, but the limiting values of activation energy in the peraluminous field are lower at lower silica content (Fig. 7b,c).

In contrast, data from the Mg-bearing systems indicate that activation energy shows little variation (Fig. 7d–f), with a slight tendency to increase with decreasing Mg/(Mg + 2Al). The measurements on the MAS67 series have more scattered values of activation energy but the origin of this is unknown. It is also of note that values of activation energy to viscous flow decrease with decreasing silica content and that the magnitudes of activation energy in the calcium and magnesium systems at the same silica content are similar.

4. DISCUSSION

4.1. Structural Implications

4.1.1. Viscosity as a probe of melt structure

As discussed by Bottinga et al. (1995), in the range 1–1000 Pa s, viscosity may be considered a reflection of the average bond strength of the melt; melts with stronger bonds having higher viscosity at a given temperature. Assuming this to be the case implies that variations in viscosity as a function of composition may be used to provide constraints on melt structure. Indeed, this approach has been employed in the past with considerable success. For example, viscosity measurements in the system Na_2O-Al_2O_3-SiO_2-P_2O_5 have been used to predict that the average Na/P ratio of phosphate complexes present in these liquids is 1.35 ± 0.07 (Toplis and Dingwell, 1996),

Table 4. Fits of viscosity data to the Arrhenian equation (see text for details)

Composition	A[a]	$B/10^4$ [a]	Activation energy[a] (kJ/mol)	Reduced activation energy[b]
CAS75a:61	−7.502	1.758	336.6	326.1[c]
CAS75a:58	−8.068	1.869	357.9	341.6
CAS75a:56	−8.265	1.913	366.2	349.3
CAS75a:54	−8.390	1.942	371.8	354.0
CAS75a:53	−8.567	1.977	378.5	360.1
CAS75a:50	−8.665	2.002	383.2	362.4
CAS75a:49	−8.809	2.027	388.0	367.4
CAS75a:47	−8.821	2.030	388.5	368.0
CAS75a:45	−8.916	2.048	392.1	371.0
CAS75a:44	−8.958	2.052	392.9	371.6
CAS75a:41	−8.417	1.952	373.8	373.8
CAS75b:55	−7.737	1.823	349.1	349.6[c]
CAS75b:53	−7.886	1.856	355.3	355.3
CAS75b:52	−7.933	1.867	357.4	357.7
CAS75b:51	−7.990	1.878	359.6	358.1
CAS75b:50.5	−8.062	1.894	362.6	363.0
CAS75b:50	−8.107	1.900	363.8	362.9
CAS75b:49	−8.189	1.916	366.9	365.5
CAS75b:47.5	−8.433	1.959	375.1	368.4
CAS75b:46	−8.513	1.976	378.2	371.2
CAS75b:43.5	−8.564	1.984	379.9	372.8
CAS67a:57	−8.709	1.867	357.5	328.0[d]
CAS67a:54	−9.023	1.931	369.6	337.9
CAS67a:52	−9.166	1.960	375.3	344.1
CAS67a:50	−9.312	1.987	380.4	346.6
CAS67a:47	−9.432	2.011	385.0	351.5
CAS67a:46	−8.828	1.902	364.1	352.8
CAS67a:41	−8.388	1.817	347.9	355.3
CAS67b:55	−8.415	1.820	348.4	334.2[d]
CAS67b:53	−9.031	1.935	370.5	336.7
CAS67b:52	−8.770	1.889	361.6	340.4
CAS67b:51	−9.081	1.943	371.9	340.4
CAS67b:50	−8.890	1.914	366.4	344.1
CAS67b:49	−9.229	1.971	377.2	346.6
CAS67b:48	−8.982	1.930	369.4	346.6
CAS50:61	−7.679	1.483	283.8	244.5[c]
CAS50:57	−8.516	1.649	315.7	265.4
CAS50:54	−8.743	1.697	324.9	273.3
CAS50:52	−8.439	1.646	315.1	277.2
CAS50:50	−8.147	1.597	305.7	278.5
CAS50:48	−7.906	1.554	297.5	281.1
CAS50:46	−7.473	1.475	282.4	282.4
CAS50:45	−7.105	1.405	269.0	
CAS50:44	−6.770	1.341	256.7	
CAS50†:57	−28.370	4.442	850.4	
CAS50†:54	−27.661	4.397	841.9	
CAS50†:52	−29.467	4.627	885.8	
CAS50†:50	−32.517	5.005	958.1	
CAS50†:48	−33.527	5.148	985.5	
CAS50†:46	−31.027	4.848	928.1	
CAS50†:45	−29.517	4.671	894.2	
MAS75:58	−7.535	1.770	338.9	341.5[f]
MAS75:57	−7.225	1.711	327.6	
MAS75:55	−7.715	1.804	345.4	343.2
MAS75:53	−7.651	1.787	342.2	345.0
MAS75:51	−7.648	1.784	341.6	343.6
MAS75:49	−7.687	1.786	342.0	344.4
MAS75:46	−7.746	1.794	343.4	346.1
MAS67a:53	−8.508	1.807	345.9	319.9[g]
MAS67a:50	−8.296	1.768	338.4	321.2
MAS67a:48	−8.096	1.730	331.2	323.1
MAS67a:46	−7.907	1.694	324.4	324.4
MAS67a:44	−7.979	1.704	326.3	326.3
MAS67b:58	−7.846	1.688	323.2	306.0[g]
MAS67b:58	−7.878	1.694	324.3	307.8

Table 4. (Continued)

Composition	A[a]	B/10[4] [a]	Activation energy[a] (kJ/mol)	Reduced activation energy[b]
MAS67b:56	−7.945	1.707	326.9	311.0
MAS67b:53	−7.971	1.709	327.3	309.8
MAS67b:50	−8.081	1.727	330.6	313.0
MAS67b:48	−7.914	1.698	325.0	316.8
MAS67b:46	−7.730	1.661	318.1	318.1
MAS50:55a	−7.205	1.388	265.8	252.4[e]
MAS50:55b	−7.192	1.386	265.3	253.7
MAS50:54	−7.221	1.392	266.5	252.4
MAS50:52	−7.213	1.390	266.1	256.3
MAS50:50	−7.042	1.359	260.1	257.6
MAS50:49	−7.008	1.352	258.9	258.9
MAS50:47	−6.889	1.329	254.5	
MAS50:44	−6.710	1.294	247.8	
MAS50†:55	−30.020	4.507	862.8	
MAS50†:52	−30.017	4.528	866.9	
MAS50†:50	−30.631	4.608	882.1	
MAS50†:49	−31.366	4.697	899.3	
MAS50†:47	−32.372	4.820	922.8	
MAS50†:45	−32.145	4.803	919.5	
MAS50†:44	−31.371	4.837	926.0	

[a] Parameters derived from fitting all available high-viscosity data (shown in Table 2) to an equation of the form: $\log_{10}\eta = A + B/T$ where η is viscosity in Pa s and T is temperature in K. For CAS50:x and MAS50:x the low-temperature data (shown in Table 3) have also been fitted to the same equation and are distinguished by the symbol †. Activation energy calculated from parameter B shown in this table.

[b] Reduced activation energy is that calculated from fitting viscosity data to the Arrhenius equation over a temperature range which is the same for all members of a given compositional series. Only in this way can the true compositional dependence of activation energy be assessed (see text for details). The exact temperature ranges are shown below.

[c] 1600–1450°C.

[d] 1550–1500°C.

[e] 1600–1550°C.

[f] 1620–1500°C.

[g] 1600–1500°C.

values in excellent agreement with those determined independently from NMR spectra of the same glasses (1.32 ± 0.10; Toplis and Schaller, 1998). A similar approach was also used for liquids close to the metaluminous join in the system Na_2O-Al_2O_3-SiO_2, based upon which it was inferred that liquids with Na/Al = 1 may contain some NBO (Toplis et al., 1997). It is also of note that this approach provides in situ measurements in the liquid at temperatures well above the glass transition, in contrast to the majority of spectroscopic studies which characterise glasses, whose structure represents that of the liquid at the glass transition temperature.

To infer structural information from our viscosity data, we will begin by considering the factors that affect average bond strength, then construct a theoretical model for quantifying the variation of average bond strength as a function of composition. As described below, the model may be fit to experimental data using two adjustable parameters, both of which have some physical or thermodynamic significance. The 'best-fit' values of these parameters will then be considered and interpreted in terms of melt structure. We begin by considering the factors that affect average bond strength of the melt.

4.1.2. Average bond strength: theoretical framework

Calculating average bond strength requires three complementary pieces of information. First of all, one must identify the species present in the liquid. Secondly relative proportions of these species must be determined. Thirdly, one must attribute a bond strength to each species.

In the simple aluminosilicate silicate liquids we are dealing with here, identification of the species is relatively straightforward. For example, for compositions with $M^{2+}/2Al > 1$, we may safely assume that the liquid contains network-forming Si, metal cations in network-modifying roles (which we will call M_{NBO}), and tetrahedrally coordinated network-forming Al associated with a charge-balancing cation (which we will call $Al^{[4]}$-M). (In the equations and calculations which follow, 'M_{NBO}' actually represents $[0.5(Mg, Ca)]_{NBO}$ and '$Al^{[4]}$-M' represents $Al^{[4]}$-$(Mg, Ca)_{0.5}$.) On the other hand, even in this compositional field it is possible that Al may be incorporated without the aid of a charge-balancing cation (a species which we will call Al_{XS}) and in the peraluminous field (when $M^{2+}/2Al < 1$) we know that this must be the case. At this stage we will not worry about the details of the structural role of excess aluminium, but will limit ourselves to consideration of a generic 'Al_{XS}' which is any aluminium incorporated without an associated charge-balancing cation.

The next step is to predict the relative proportions of melt species as a function of composition across the metaluminous join. This is possible if one considers the simple chemical equilibrium:

$$Al^{[4]}\text{-}M \Leftrightarrow Al_{XS} + M_{NBO} \quad (3)$$

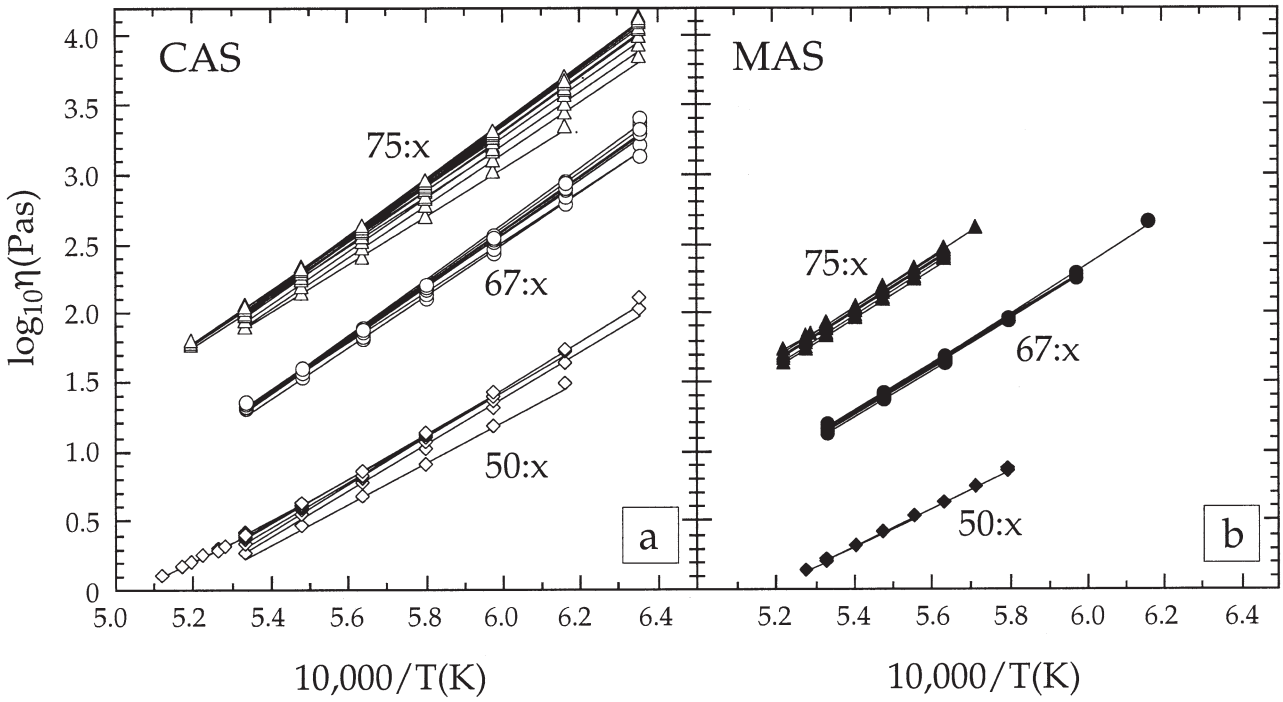

Fig. 2. Viscosities measured using the concentric cylinder technique as a function of inverse temperature for the systems $CaO-Al_2O_3-SiO_2$ (a) and $MgO-Al_2O_3-SiO_2$ (b). Triangles are data from the 75 mol.% SiO_2 isopleth, circles from the 67 mol.% SiO_2 isopleth, and diamonds from the 50 mol.% SiO_2 isopleth.

Note that silica does not appear in this equation because we are interested in variations in average bond strength along isopleths of constant silica content. In this case SiO_2 can be neglected, although in general it should be appreciated that substituting $Al^{[4]}$-M for Si will affect average bond strength and thus viscosity (Solvang et al., 2004). As with any chemical

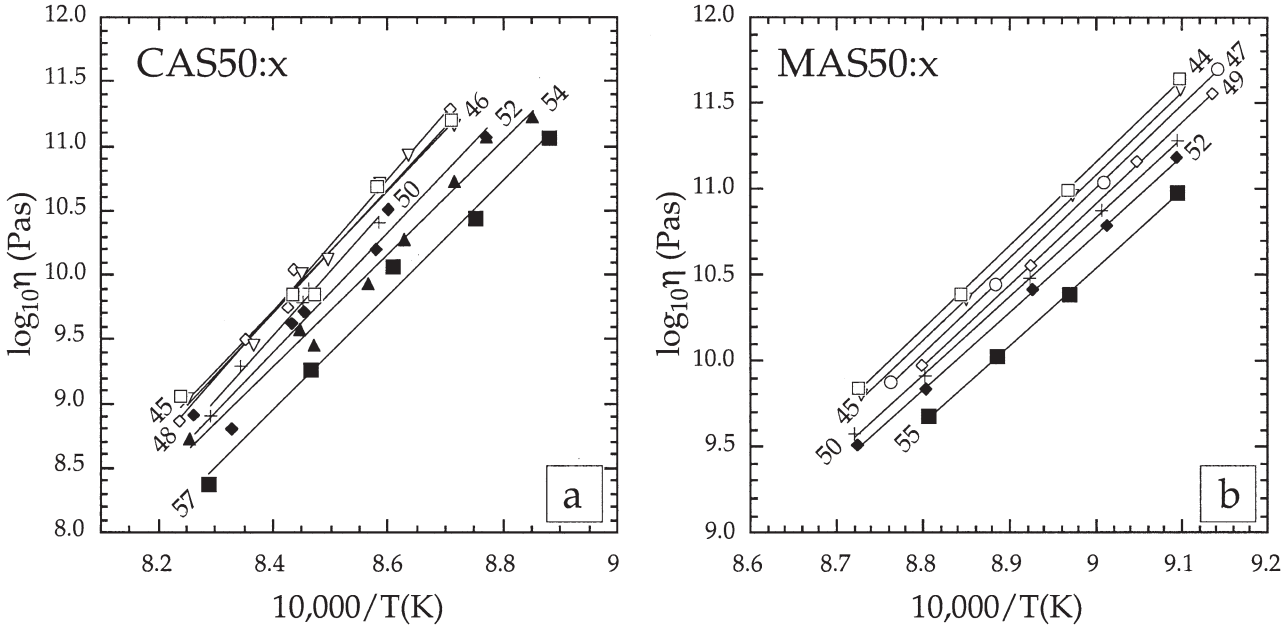

Fig. 3. Viscosities of liquids with 50 mol.% SiO_2 measured under (a) uniaxial compression (system $CaO-Al_2O_3-SiO_2$) or (b) using the micropenetration technique ($MgO-Al_2O_3-SiO_2$). Each symbol represents a composition of different $M^{2+}/(M^{2+} + 2Al)$, as indicated by values on the figure. Lines are linear regressions to the data (see text and Table 4 for details).

Table 5. Fitted parameters of combined high-and low-temperature viscosity data to the TVF equation (see text for details).

Composition	A_{TVF}	B_{TVF}	C_{TVF}
CAS50:57	−5.48 (67)[a]	6370 (910)[a]	745 (41)[a]
CAS50:54	−5.87 (63)	6910 (870)	731 (38)
CAS50:52	−5.76 (77)	6760 (1040)	743 (48)
CAS50:50	−4.85 (52)	5510 (690)	807 (34)
CAS50:48	−5.58 (52)	6530 (730)	763 (33)
CAS50:46	−6.47 (56)	7600 (860)	711 (37)
CAS50:45	−6.23 (76)	7820 (1250)	699 (54)
CAS67:50	−6.01 (64)	9100 (1070)	618 (44)
MAS50:55	−5.30 (49)	6300 (720)	713 (34)
MAS50:52	−5.72 (38)	6920 (580)	691 (26)
MAS50:50	−5.84 (25)	7130 (390)	683 (17)
MAS50:49	−5.96 (23)	7350 (380)	675 (16)
MAS50:47	−5.80 (10)	7110 (160)	688 (71)
MAS50:45	−5.81 (6)	7110 (100)	690 (4)
MAS50:44	−5.80 (8)	7110 (130)	692 (6)

[a] Numbers in parentheses correspond to uncertainties in terms of least units cited.

equilibrium, the relative proportions of the different species will be a function of the equilibrium constant, K, of the reaction, in this case defined as:

$$K = ([a\mathrm{M_{NBO}}] * [a\mathrm{Al_{XS}}])/[a\mathrm{Al^{[4]}} - \mathrm{M}] \quad (4)$$

where a represents thermodynamic activity of the relevant species which we will approximate by relative proportion. Thus, if the equilibrium constant of the reaction is known and the total number of moles of Al and M (i.e., the bulk composition) is known, then Eqn. 4 may be solved to calculate the relative proportions of the three species shown in Eqn. 3. For example, if K has a value of zero (the assumption embedded in the commonly employed 'stoichiometric' model of silicate melt structure), solution of Eqn. 4 predicts that as long as M/2Al is >1 all liquids are constituted of only M_{NBO} and $Al^{[4]}$-M, whereas for liquids with M/2Al < 1 only Al_{XS} and $Al^{[4]}$-M are present. Going across the metaluminous join from M/2Al > 1 to <1, the relative proportion of $Al^{[4]}$-M reaches a maximum when M/2Al = 1, at which point it is the only species present in the liquid (see Fig. 8). However, if one considers a value of the equilibrium constant greater than zero, solution of Eqn. 4 implies that Al_{XS} will begin to appear even in compositions with M/2Al > 1, that M_{NBO} will persist into the peraluminous field, and that liquids with M/2Al = 1 will contain a mixture of all three species, M_{NBO} and Al_{XS} occurring in equal proportions. This is illustrated in Figure 8 for K = exp(−5).

To complete our discussion of average bond strength we need to consider the relative bond strengths of each of the species present in Eqn. 3. In this respect, it seems entirely reasonable to assume that the average bond strength of the network-modifying M_{NBO} is less than that of the network-forming $Al^{[4]}$-M. On the other hand, the average bond strength of Al_{XS} is something of an unknown quantity and will depend on the details of the structural role of excess Al. To simplify the problem, we will consider a scale of relative bond strength from 0 to 1, in which 0 is the bond strength of M_{NBO} and 1 is that of $Al^{[4]}$-M. In this way, we do not need to worry about the absolute values, but only relative ones. If Al_{XS} has a bond strength equal to that of $Al^{[4]}$-M, then across the metaluminous join average bond strength will increase continuously, asymptotically reaching a constant value in the peraluminous field (Fig. 9). If, on the other hand, the bond strength of Al_{XS} is intermediate between those of M_{NBO} and $Al^{[4]}$-M, then for values of K > 0, average bond strength will show a maximum in the vicinity of the metaluminous join, but occurring in the peraluminous field (Fig. 9). If Al_{XS} has the same bond strength as M_{NBO}, the maximum in average bond strength will occur exactly at M/2Al = 1 and the variation will be symmetric either side of the metaluminous join, whereas if the bond strength of Al_{XS} is less than that of M_{NBO} (which will result in negative values on a scale from 0 to 1) then the maximum in average bond strength will occur in the field where M/2Al > 1, as illustrated in Figure 9.

4.1.3. Fitting experimentally determined viscosities

As may be appreciated from Figures 8 and 9, the variation of average bond strength with composition will be a function of: i) the value of K, and ii) the value of the relative bond strength of Al_{XS}. Furthermore, from standard thermodynamic relations it may be appreciated that:

$$\ln K = \Delta G_{(3)}/RT \quad (5)$$

where $\Delta G_{(3)}$ is the standard free energy of reaction 3 shown above. Thus, if temperature is known, we can consider values of free energy rather than values of K. Within the framework of Eqns. 3, 4, and 5 the experimental data at 1600°C along each isopleth in the CAS and MAS systems (Table 2; Figs. 4 and 5) have been fitted by adjusting values of $\Delta G_{(3)}$ and average bond strength of Al_{XS}.

In detail, for the fitting procedure we compare the *changes* in the *logarithm* of viscosity with changes in the logarithm of calculated bond strength. This approach has been taken because, for relatively small variations in absolute values such as those we are dealing with here along an individual silica isopleth, the variation of the logarithm of values is a measure of the *percentage* rather than the absolute change. In this way, use of the relative bond strength scale described above may be used without the need to know absolute values. In this case a constant may be added to the calculated values of log(average bond strength) to bring them into accordance with the values of log(η). Examples of resulting fits are illustrated in Figure 10 for the series CAS75 and MAS67 where experimental data are the most abundant. The fits to all compositional series are extremely satisfactory. Of particular note is the excellent agreement of modelled and experimentally determined variations for compositions with Ca/(Ca + 2Al) >0.5 in the system CAS (Fig. 10a). This compositional range is of interest because variations in calculated average bond strength are more or less independent of the values of $\Delta G_{(3)}$ and bond strength of Al_{XS} used, thus confirming the validity of our approach and the use of the relative bond strength scale.

As summarized in Table 6, the values of $\Delta G_{(3)}$ at 1600°C in the calcium-bearing system vary from −90 kJ/mol at 75 mol.% SiO_2 to −66 kJ/mol at 50 mol.% SiO_2. Values of average bond

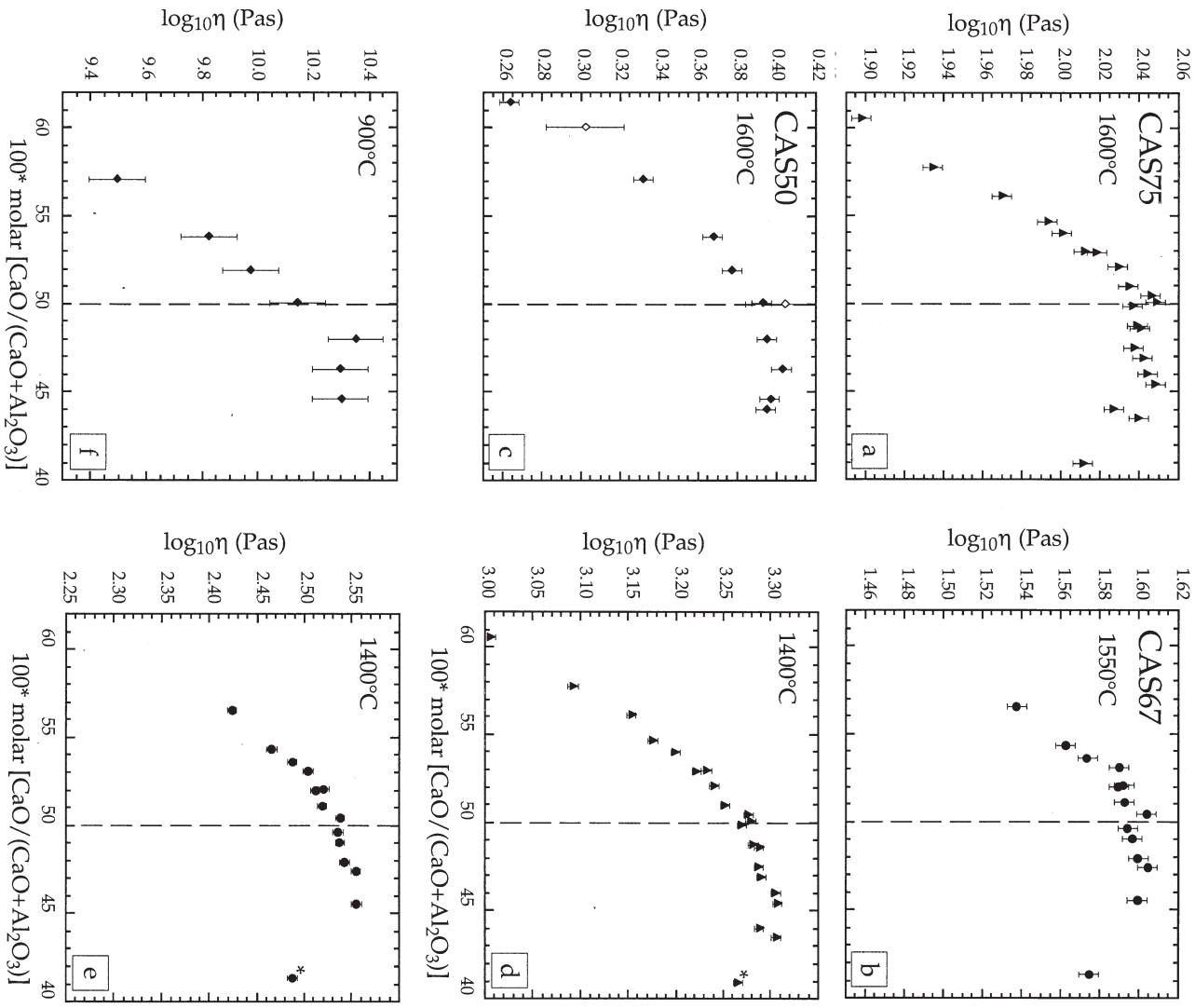

Fig. 4. Viscosities at constant temperature in the system CaO-Al_2O_3-SiO_2 as a function of $100*CaO/(CaO + Al_2O_3)$. Symbol shapes as in Figure 2. Closed symbols are data from this study, and open symbols are data from the literature (Tauber and Arndt, 1987; Urbain et al., 1982). Error bars represent experimental precision for data from this study and experimental accuracy for literature data. (a) Data at 75 mol.% SiO_2 and 1600°C; (b) 67 mol.% SiO_2 and 1550°C; (c) 50 mol.% SiO_2 and 1600°C; (d) 75 mol.% SiO_2 and 1400°C; (e) 67 mol.% SiO_2 and 1400°C; (f) 50 mol.% SiO_2 and 900°C. All data represent direct measurements except values shown on (f), which are viscosities interpolated to 900°C using fits to Eqn. 1, and values shown by an asterisk which are values extrapolated using fits to Eqn. 1 (Table 4).

strength of Al_{XS} are about halfway between those of network-forming $Al^{[4]}$-M and Ca_{NBO} with no systematic variation as a function of silica content. In the magnesian system, values of $\Delta G_{(3)}$ at 1600°C and Al_{XS} both contrast strongly with values in the calcium-bearing system, $\Delta G_{(3)}$ having positive, albeit small, values, while the bond strength of Al_{XS} is predicted to be approximately that of Mg_{NBO}. The potential roles of Al_{XS} and the structure of our studied liquids will be discussed in terms of the values shown in Table 6.

4.1.4. Structural implications

In the literature two possibilities have been suggested for the structural role of Al_{XS}. The first involves incorporation of Al through association with an oxygen in threefold coordination in a structure called a tricluster (Lacy, 1963). In this case, Al remains in tetrahedral coordination and maintains a network-forming character. We note in passing that three different Al-bearing triclusters are possible, depending on the number of Al involved (1, 2, or 3), the other bonds to oxygen being associated with silicate tetrahedra (Toplis et al., 1997; Stebbins et al., 2001). The second way to incorporate excess Al is as a network-modifier (Mysen et al., 1981), in which case Al_{XS} will have a coordination number greater than 4, but which could be 5 and/or 6 (Poe et al., 1992; Sato et al., 1991). Given simple bond valence and bond length arguments, triclusters would be expected to have a relatively high average bond strength

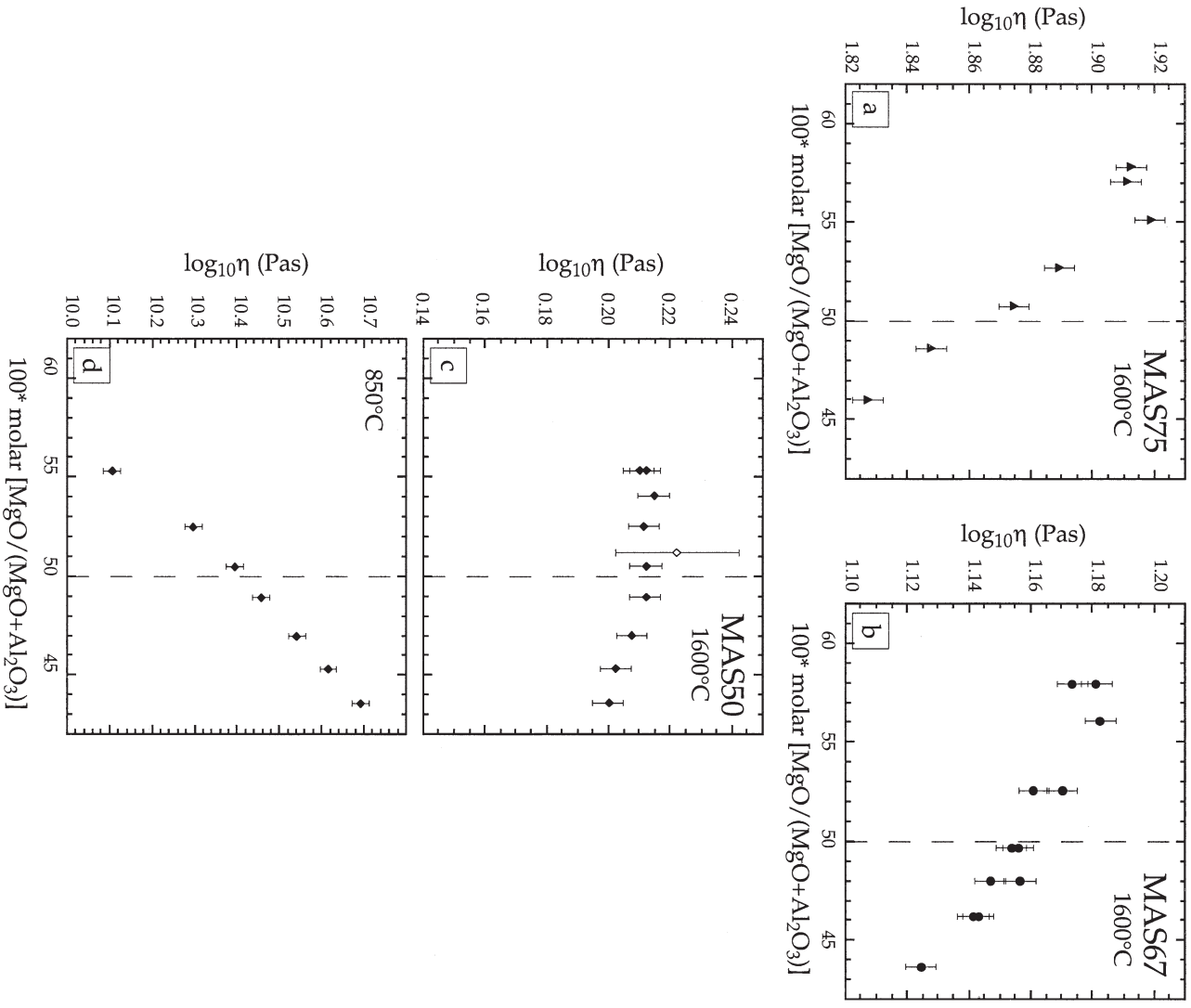

Fig. 5. Viscosities at constant temperature in the system MgO-Al_2O_3-SiO_2 as a function of 100*MgO/(MgO + Al_2O_3). Symbol shapes as in Figure 2. Closed symbols are data from this study, and open symbol represents data of Riebling (1964) at 50 mol.% SiO_2. Other data of Riebling (1964) at higher values of 100*MgO/(MgO + Al_2O_3) clearly indicate a maximum in viscosity. Error bars represent experimental precision for data from this study and experimental accuracy for literature data. (a–c) Data at 1600°C along the 75, 67, and 50 mol.% SiO_2 isopleths respectively. (d) 50 mol.% SiO_2 and 850°C. All data represent direct measurements except values shown on (d), which are viscosities interpolated using fits to Eqn. 1 (Table 4).

whereas high coordinated Al may be expected to have a strength comparable, or even lower than that of M_{NBO}.

In light of this, the fitted values of the average bond strength for Al_{XS} in CAS liquids would appear consistent with triclusters as the dominant form of Al_{XS} in our liquids, although we cannot exclude the presence of some high-coordinate Al (Stebbins et al., 2000), nor predict what may happen in more peraluminous compositions (Sato et al., 1991). Concerning the existence of triclusters in our liquids, we note that such structures have been shown to be dynamically stable in the system CAS (e.g., molecular orbital calculations of Kubicki and Toplis, 2002) and are predicted to occur in significant concentrations in molecular dynamic simulations of calcium aluminosilicate liquids (Nevins and Spera, 1998; Morgan and Spera, 2001; Benoit et al., 2001). Spectroscopic data also support this hypothesis. For example, in anorthite glass there is evidence for ~5% of nonbridging oxygens (Stebbins and Xu, 1997) but no evidence for more than 1% of high coordinate Al (Baltisberger et al., 1996; Stebbins et al., 2000). If the NBO are not associated with Al, then they are most reasonably associated with Ca, in turn implying the presence of triclusters (cf. Eqn. 3). In this respect, it is of note that we may predict the number of NBO in anorthite liquid at 1600°C using the value of $\Delta G_{(3)}$ fitted to our viscosity data (Table 6) and Eqn. 4. A value of 3.8% of total oxygens as NBO is calculated, in good agreement with the value measured by ^{17}O NMR (Stebbins and Xu, 1997). Fur-

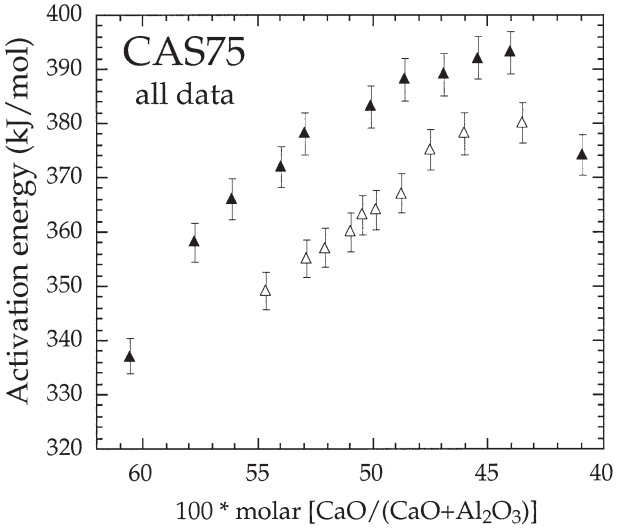

Fig. 6. Activation energy to viscous flow for compositions in the system $CaO-Al_2O_3-SiO_2$ at 75 mol.% SiO_2 calculated using all the concentric cylinder measurements of this study. Open symbols are data from series 'a' and closed symbols from series 'b'. Error bars represent estimated uncertainty of ±1%.

thermore, the values of $\Delta G_{(3)}$ derived from the viscosity data are comparable to enthalpies of formation of triclusters in calcium-bearing melts predicted by Kubicki and Toplis (2002). Finally, in situ high-temperature Raman spectra of anorthite liquid (Daniel et al., 1995) show that there are temperature-dependent changes in the Raman spectrum above the glass transition and that the frequencies at which these changes occur are indicative of subtle changes in the stretching vibrations of bridging oxygens, exactly what would be expected if triclusters are being formed. It is also of note that no spectral changes associated with the formation of high coordinate Al were observed (Daniel et al., 1995).

As discussed above, three different triclusters of variable Si/Al may exist. In the system $Na_2O-Al_2O_3-SiO_2$ the viscosity data of Toplis et al. (1997) showed that position of the viscosity maximum is a systematic function of silica content, showing greatest offset from the join Na/Al = 1 at 67 mol.% SiO_2. This observation may be simply explained if triclusters involving only one Al dominate at all silica contents, as discussed by Toplis et al. (1997). However, in the system $CaO-Al_2O_3-SiO_2$ there is no systematic shift in the position of the viscosity maximum as a function of silica content (Fig. 4). This observation implies that there is no single tricluster species which dominates in all liquids, but may be explained if the average number of Al per tricluster is a function of silica content (e.g., variable relative proportions of triclusters associated with 1, 2 and/or 3 Al). Indeed, this would explain why values of $\Delta G_{(3)}$ and bond strength of Al_{XS} vary as a function of silica content (Table 6). In this respect, we note that confirmation of the presence or absence of triclusters with 1 and/or 2 Al in anorthite glass using ^{17}O NMR is probably not possible, because the peaks associated with these environments overlap those of the dominant bridging oxygen environments Si-O-Al and Si-O-Si (Kubicki and Toplis, 2002). The same problem is encountered at lower silica content where the peak associated with triclusters surrounded by 3 Al overlaps that of the Al-O-Al environment (Stebbins et al., 2001). Thus, further spectroscopic and theoretical studies are required to quantify the relative proportions of triclusters and to constrain their possible temperature dependence.

Another point of note is that the activation energy to viscous flow is almost perfectly inversely proportional to the relative proportion of M_{NBO} (i.e., both show the same variation as a function of Ca/(Ca + 2Al) as shown in Figs. 7 and 8). This is consistent with a central role of NBO in the viscous flow mechanism of deploymerised liquids, in agreement with previous studies (Stebbins, 1991; Toplis, 1998). In peraluminous liquids where the number of NBO becomes vanishingly small, it is possible that triclusters may play an intermediate role analogous to that inferred for fivefold coordinated silicon and/or aluminium in depolymerised compositions (Stebbins, 1995), and that the activation energy in the peraluminous field is related to the energy of the formation and destruction of such species.

Turning now to the system $MgO-Al_2O_3-SiO_2$, we note that the values of $\Delta G_{(3)}$ and average bond strength of Al_{XS} inferred from viscosity measurements are very different from those derived from the calcium-bearing system (Table 6). The inferred average bond strength of Al_{XS} is almost identical to that of Mg_{NBO}, pointing to a network-modifying role of Al_{XS} in these liquids. Indeed, NMR studies of $MgO-Al_2O_3-SiO_2$ glasses similar or identical to those studied here show clear evidence for a population of Al in fivefold coordination (McMillan and Kirkpatrick, 1992; Toplis et al., 2000) in support of this conclusion. However, in the peraluminous *glasses* studied by Toplis et al. (2000) it is found that the observed number of Al^5 is not sufficient to account for the stoichiometric excess of Al over Mg, thus $Al^{[4]}$ associated with triclusters may also be present. However, it is possible that at 1600°C liquid structure is different from that at the glass transition. Indeed, one of the striking features of the MAS data (compared to data from the corresponding Na or Ca bearing systems) is that the variation of viscosity across the metaluminous join at temperatures close to the glass transition is very different from that at 1600°C (Fig. 5c,d), consistent with a significant temperature dependence of liquid structure. We note that both molecular dynamics simulations and spectroscopic study of highly peraluminous liquids inply that the formation of high-coordinated aluminium species is favoured with increasing temperature (Poe et al., 1992), thus it is possible that such species dominate in Mg-bearing liquids at 1600°C, although further spectroscopic data are required to confirm this conclusion.

The other striking feature of the data in the MAS system is that derived values of $\Delta G_{(3)}$ are systematically close to zero, implying that Al has no thermodynamic preference to be charge-balanced by Mg. We note that this conclusion would be compromised if Eqn. 3 did not describe the components present in the liquid, for example, if a proportion of Mg were tetrahedrally coordinated. In this case the number of Mg_{NBO} for a given bulk composition would be smaller than predicted and a maximum in viscosity in the field of Mg/2Al > 1 would be

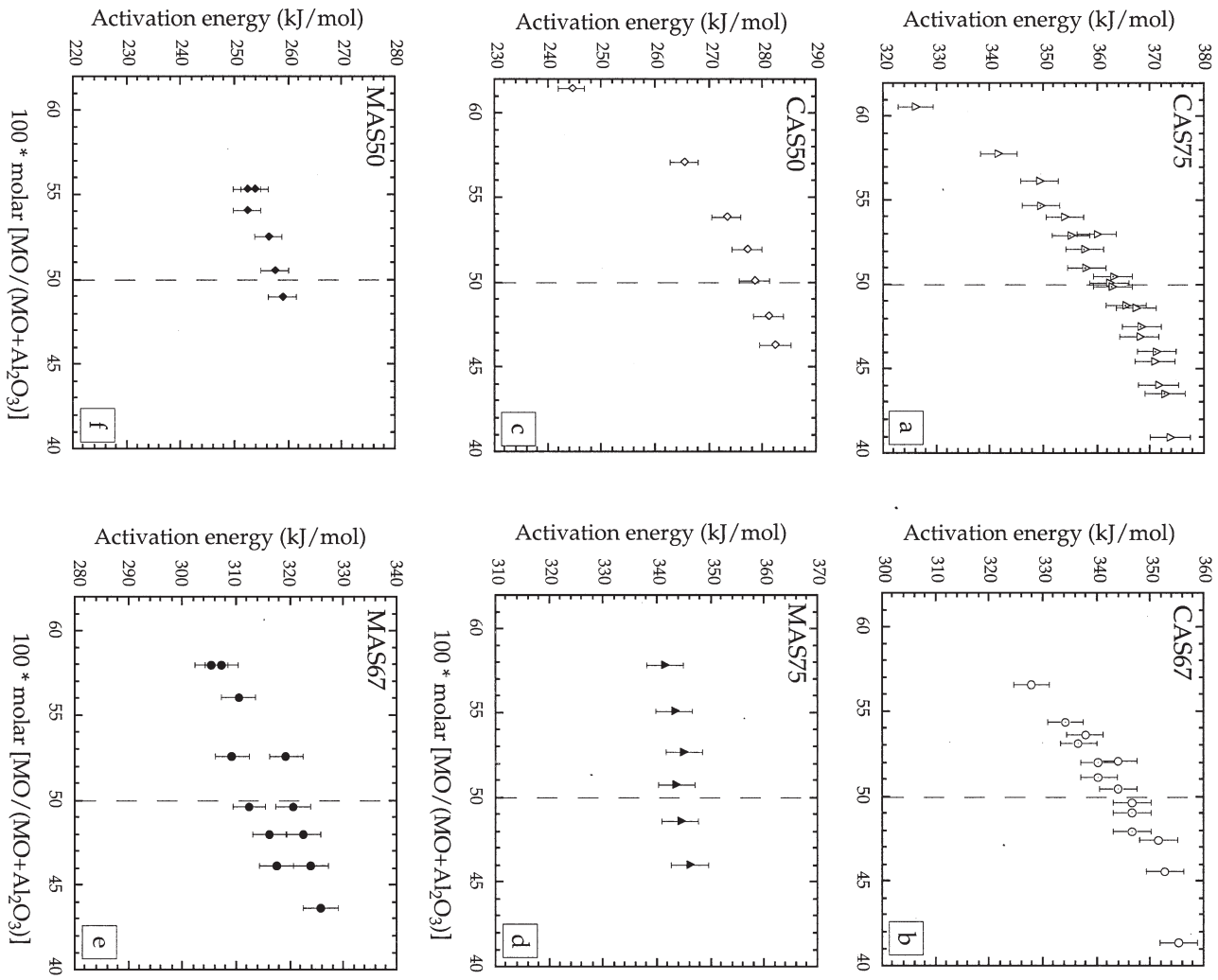

Fig. 7. Activation energy to viscous flow calculated using only data over an identical range of temperature for each compositional series, as detailed in Table 4. Symbols as in Figure 2. For Ca-bearing compositions open symbols are series 'a' and symbols with a dot are series 'b'.

possible. However, in this case, the viscosity maximum should occur closer to the metaluminous join at 75 mol.% SiO_2 than at 50 mol.% SiO_2, but this would not appear to be the case (Fig. 5). Moreover, although some X-ray scattering studies have inferred that Mg may occur in tetrahedral coordination in silicate glasses and liquids, such results are controversial (Brown et al., 1995) and NMR data suggest that Mg is octahedrally coordinated in simple silicate glasses (Fiske and Stebbins, 1994). We therefore prefer the interpretation that Al has no thermodynamic preference to be charge-balanced by Mg. Indeed, several other independent lines of evidence suggest that this may be the case. The most direct evidence is the thermochemical data of Roy and Navrotsky (1984) which show that enthalpies of mixing along the join SiO_2-$MgAl_2O_4$ are close to zero, consistent with no significant association of Mg and Al. Further support is provided by square-wave voltammetry measurements of liquids in the temperature range 1300 to 1600 °C (Wiedenroth and Rüssell, 2003). In that study (of the system Na_2O-MgO-CaO-Al_2O_3-SiO_2), it was found that the standard reduction potential of trace amounts of iron showed maximum values when $(Na_2O + CaO)/Al_2O_3 = 1$, but not when $(Na_2O + CaO + MgO)/Al_2O_3 = 1$, an observation interpreted to imply that Mg does not charge balance tetrahedrally coordinated Al^{3+} in those liquids. We note too that Mysen et al. (1980) reached an analogous conclusion concerning the (in) ability of Mg to stabilise Fe^{3+} in tetrahedral coordination. Therefore, in conclusion there is evidence that in the system MAS, Al_{XS} is incorporated as a network-modifier and that it may occur in abundance, even in liquids with $Mg/2Al > 1$.

To summarise, the results presented here combined with those of Toplis et al. (1997) imply that the structure of ternary aluminosilicate liquids close to the charge-balanced join is sensitive to the identity of the low field strength metal cation present. These differences involve both the degree of departure from the classical model of silicate melt structure (these departures being greatest when Mg is the metal cation and smallest when Na is the metal cation) as well as the structural role of Al_{XS} (exclusively triclusters for Na-bearing liquids, dominantly

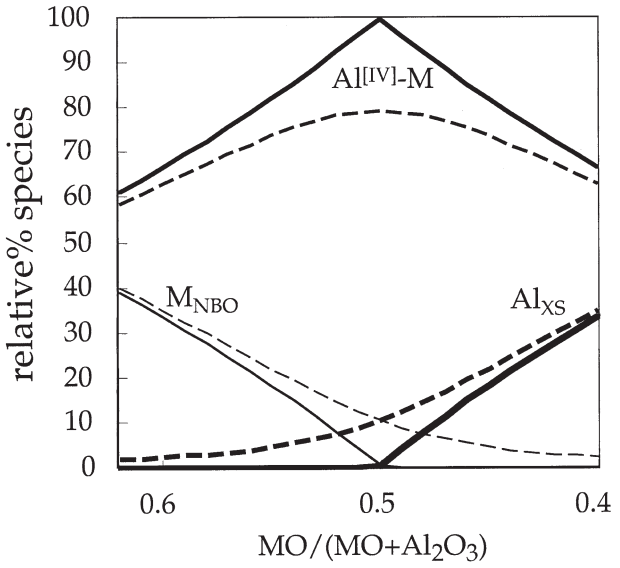

Fig. 8. Theoretical variations of the relative proportions of the three species of Eqn. 3 as a function of $M^{2+}O/(M^{2+}O + Al_2O_3)$. Solid lines are values calculated assuming that the equilibrium constant of Eqn. 3 (K) is 0; dashed lines are values calculated with $\ln K = -5$.

triclusters for Ca-bearing liquids, and dominantly high coordinate Al for Mg-bearing liquids). The degree of departure from the classical model of melt structure (i.e., the equilibrium constant of Eqn. 3) is a reflection of the stability of charge-balanced Al in tetrahedral coordination and may be rationalised in terms of relative energetic stabilities determined by Roy and Navrotsky (1984). On the other hand, although the structural role of Al_{XS} also appears to be related to the field strength of

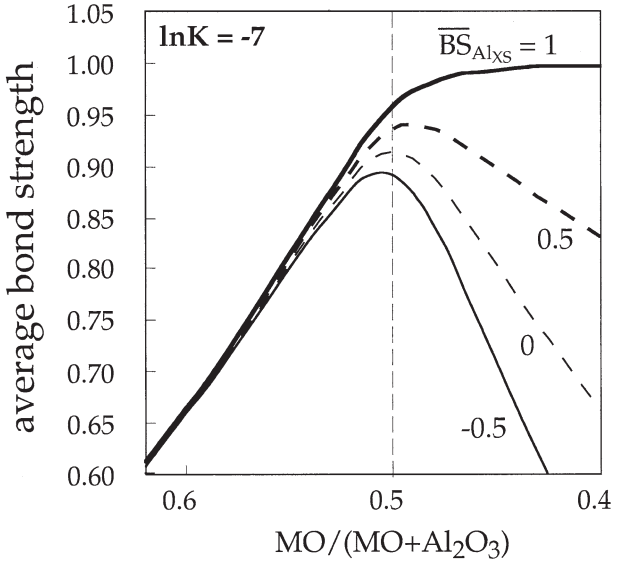

Fig. 9. Theoretical variation of average bond strength as a function of $M^{2+}O/(M^{2+}O + Al_2O_3)$ assuming different bond strengths of Al_{XS} relative to $Al^{[4]}$-M and M_{NBO}, as discussed in the text. For example, thick solid line is bond strength of Al_{XS} identical to that of $Al^{[4]}$-M (1), and thin dashed line a bond strength of Al_{XS} identical to that of M_{NBO} (0).

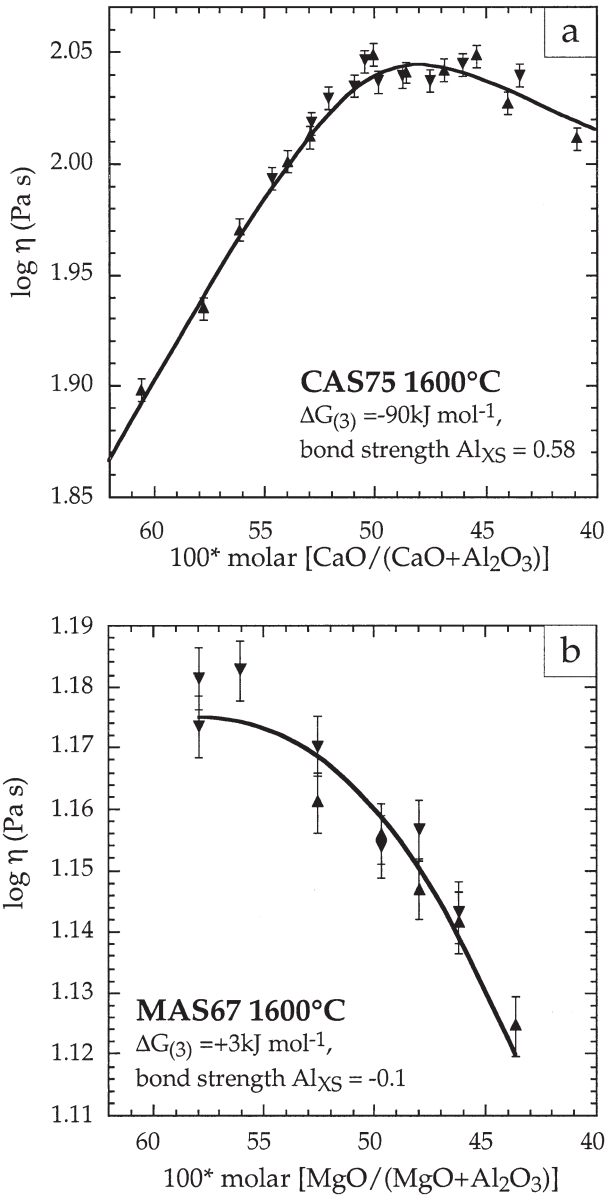

Fig. 10. Examples of fits of viscosity data at 1600°C using parameters of Eqns. 3, 4, and 5 for compositional series (a) CAS75 and (b) MAS67. A complete summary of best fit parameters is shown in Table 6.

the metal cation, further work is required to understand the detailed roles of cation charge and cation size on the relative stabilities of triclusters and high coordinate Al.

4.2. Implications for the Polymerisation State of Silicate Liquids

As mentioned above, many physical and thermodynamic properties show smooth variations when plotted as a function of 'NBO/T', and the use of NBO/T as a quantitative measure of the polymerisation state of the liquid is becoming more widespread. However, in light of the results and discussion above it

Table 6. Values of variables in Equations 3, 4, and 5 (see text for details) used to fit viscosity data at 1873K.

Series	$\Delta G_{(3)}$ at 1873K (kJ/mol)	InK	Bond strength Al_{XS}
CAS75	−90	−5.79	+0.58
CAS67	−76	−4.88	+0.42
CAS50	−66	−4.27	+0.45
MAS75	+8	+0.49	−0.11
MAS67	+3	+0.19	−0.08
MAS50	+0.2	+0.01	+0.03

is clear that values of NBO/T calculated assuming that all Al is associated with metal cations may not be a true reflection of the polymerisation state. This in turn may be important when constructing models to describe the compositional dependence of physical and thermodynamic parameters. In the next section we will quantify the real values of NBO/T for the liquids studied here, then qualitatively discuss the implications of our results for natural silicate liquids of interest to the earth sciences.

4.2.1. In the systems CAS and MAS

As described earlier, if values of $\Delta G_{(3)}$ are known, we can quantify the relative proportions of M_{NBO}, Al_{XS}, and $Al^{[4]}$-M as a function of composition. Furthermore, if an assumption is made about the structural role of Al_{XS}, the total number of NBO (to M and possibly Al) and the number of tetrahedral cations may be quantified, allowing real values of NBO/T to be calculated. These values may then be compared with those calculated assuming that, wherever possible, Al is charge-balanced by Ca or Mg (which we will call the nominal values).

For example, in the calcium-bearing system we will assume that Al_{XS} is incorporated in triclusters, such that Al remains in tetrahedral coordination and that there are no NBO associated directly with Al. In this case there is good first-order agreement between real and nominal values of NBO/T (Fig. 11a), although in detail discrepancy increases with decreasing silica content at a given Ca/2Al, and as Ca/2Al approaches 1 for a given silica content (Fig. 11a). The real value of NBO/T in anorthite liquid is predicted to be 0.08 compared to the nominal value of zero. This corresponds to a little less than 4% of all oxygens as NBO, as mentioned previously. The calculated offset is greatest along the 50 mol.% SiO_2 isopleth because these liquids are richer in Al at a given Ca/(Ca + 2Al) and also because the estimated value of $\Delta G_{(3)}$ is less negative than at higher silica content.

The offsets of real NBO/T from nominal values are considerably more dramatic in the magnesium-bearing system (Fig. 11b). In this case it has been assumed that Al_{XS} is not tetrahedrally coordinated, and that Al_{XS} creates additional NBO. Because the number of NBO associated with Al_{XS} is not known with certainty, we illustrate values of NBO/T calculated assuming 1 and 3 NBO per Al_{XS} (Fig. 11b). In both cases calculated values of NBO/T are significantly higher than the nominal ones, this offset being greater at lower silica content in each case. For the case of 1NBO per Al_{XS}, NBO/T is predicted to vary little along a given silica isopleth, whereas if 3NBO per

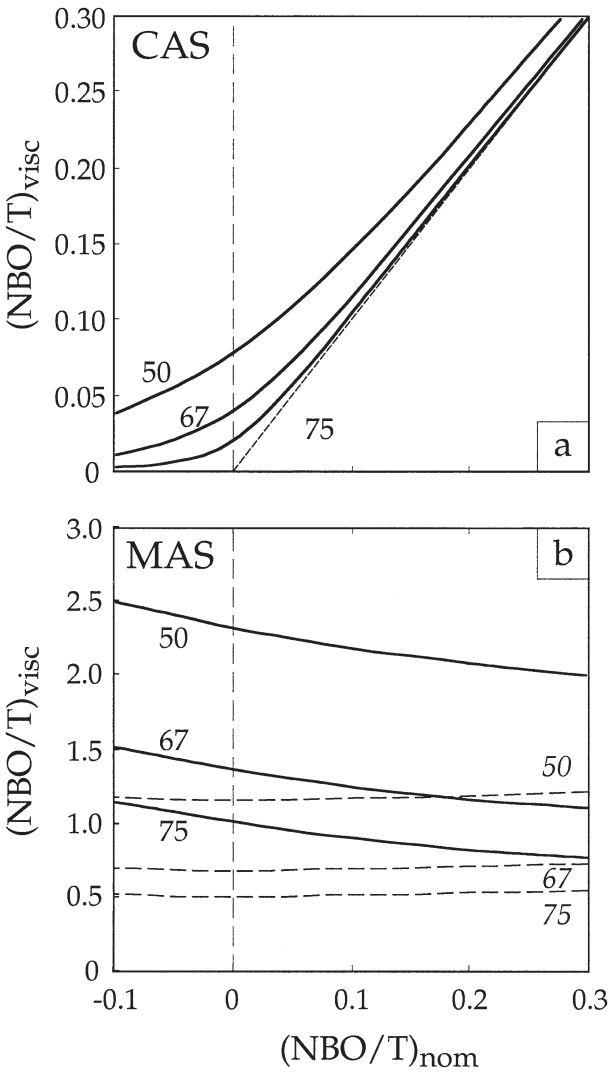

Fig. 11. NBO/T calculated assuming that all Al is associated with charge-balancing cations (NBO/T_{nom}) compared to values calculated using fit parameters to the viscosity data (NBO/T_{visc}). In the peraluminous field the deficit in metal cations is expressed as a negative number of NBO when calculating NBO/T_{nom}. (a) For the system CaO-Al_2O_3-SiO_2, calculation of (NBO/T_{visc}) is made assuming that Al_{XS} is in triclusters, with all Al in tetrahedral coordination and no NBO associated directly with Al. The thin dashed line is 1:1. Numbers indicate the silica content. (b) For the system MgO-Al_2O_3-SiO_2, NBO/T_{visc} is calculated assuming that Al_{XS} is not in tetrahedral coordination. Solid lines represent values of NBO/T_{visc} assuming that each Al_{XS} creates 3 NBO and dashed lines assuming 1 NBO. Numbers indicate silica content, in italics for the case of 1NBO per Al_{XS}.

Al_{XS} are assumed then liquids are predicted to become more *depolymerised* as the metaluminous join is approached. In this latter case, the real value of NBO/T in the magnesian equivalent of anorthite liquid is predicted to be 2.3 compared to the nominal value of zero, and ~65% of all oxygens are predicted to be NBO (rather than zero!). In summary, the real polymerisation state of Mg-bearing liquids is very different from that predicted assuming that Mg charge balances Al, being significantly more depolymerised in all cases.

4.2.2. In natural systems

The results presented herein have some bearing on the compositions of natural granitic systems which have nominal NBO/T close to zero and which may even be peraluminous. Although these liquids are generally rich in alkalies rather than alkaline earths, the results presented here and those of Toplis et al. (1997) may be used to infer that the number of NBO may be greater than expected and that any Al_{xs} present will most likely remain in tetrahedral coordination in some sort of tricluster.

Another field of application is Mg-rich liquids produced by partial melting of the mantle. Such liquids are generally depolymerised, but in light of the results above it is of interest to consider whether they are not in fact more depolymerised than expected. This will potentially be the case if the molar ratio $(Na_2O + K_2O + CaO)/Al_2O_3 < 1$, such that a proportion of the aluminium remains to be charge-balanced. To assess this possibility, we have concentrated on experimentally produced liquids, first of all because they represent a wider range of composition than lavas erupted and sampled at the Earth's surface, and secondly because reported compositions are unambiguously those of liquids, which is not always the case of whole rock analyses. Consideration of available data shows that despite being the richest in MgO, liquids produced by high degrees of melting at high pressure (Walter, 1998) never have molar $(Na_2O + K_2O + CaO)/Al_2O_3 < 1$, mainly because Al_2O_3 contents are not particularly high. On the other hand, certain liquids relevant to Mid-Ocean Ridge Basalt petrogenesis, produced by partial melting of peridotite at 1 GPa, do have $(Na_2O + K_2O + CaO)/Al_2O_3 < 1$. Of particular note are liquids produced by extensive melting of source compositions poor in clinopyroxene (Pickering-Witter and Johnston, 2000; Schwab and Johnston, 2001) and those produced by small degree melting of fertile mantle at low pressure (Baker et al., 1995). In both of these cases it is the high concentrations of Al_2O_3 which lead the ratio $(Na_2O + K_2O + CaO)/Al_2O_3$ to be close to or less than 1, and it is possible that in these cases a proportion of Al may be in a network-modifying role rather than associated with Mg. Another family of natural liquids which may be concerned are high-Mg andesites, in particular low-Ca boninites. Indeed, consideration of glass compositions reported by Ohnenstetter and Brown (1996) shows that on an anhydrous basis the ratio $(Na_2O + K_2O + CaO)/Al_2O_3$ is significantly less than 1, although the role of water clearly must also be taken into account when calculating the polymerisation state. In conclusion, it is likely that diverse natural liquids may have a structure and polymerisation state somewhat different from that predicted by simply assuming that all Al is associated with charge-balancing cations. In these cases 'real' values of NBO/T will be higher than expected because a proportion of Al may be present in network-forming triclusters and/or a network-modifying high coordination state.

5. CONCLUDING REMARKS

In light of the results presented above, one should be aware that the calculation of the polymerisation state of silicate liquids must be treated with caution, whether in simplified 'analog' systems such as anorthite–diopside, or in natural systems. Furthermore, it should be appreciated that the deviations of NBO/T from nominal values is a complex function of the composition of the liquid, in particular the nature of the monovalent and divalent metal cations. We also note that the above work relates only to a pressure of one atmosphere and that natural liquids, which are often produced and transported at depth, are equilibrated at higher pressures. For example, high coordinate Al is known to be favoured at high pressure (Yarger et al., 1995). As a further complication, studies of amorphous silicates at high pressure have also proposed hybrid structures which involve both high coordinate Al and triclusters (Daniel et al., 1996; Poe et al., 2001). We therefore conclude that there is a need for more spectroscopic information, particularly at high pressure, but we note that the data presented here provide a stringent test of any structural models at one atmosphere and constitute a necessary starting point for studies at higher pressure.

Acknowledgments—This work grew out of collaboration between M.J.T. and D.B.D. while at the Bayerisches Geoinstitut, Bayreuth, Germany. During the early stages of this work, financial support was provided by the European Union, both through a Marie Curie fellowship to M.J.T. as well as the EU "IHP–Access to Research Infrastructures" Programme (Contract No. HPRI-1999-CT-00004 to D. C. Rubie). Conrad Gennaro is thanked for completing measurements of the CAS50 series using the micropenetration technique, and Pascal Richet for providing access to the experimental facilities at the IPG in Paris. Brent Poe, Pascal Richet, and Simon Kohn are thanked for informal comments, as well as three anonymous journal referees and J. K. Russell for their reviews of this work. This is CRPG contribution number 1689.

Associate editor: J. K. Russell

REFERENCES

Baker M. B., Hirschmann M. M., Ghiorso M. S., and Stolper E. M. (1995) Compositions of near-solidus peridotite melts from experiments and thermodynamic calculations. *Nature* **375,** 308–311.

Baltisberger J. H., Xu Z., Stebbins J. F., Wang S., and Pines A. (1996) Triple quantum two-dimensional ^{27}Al magic angle spinning nuclear magnetic resonance spectroscopic study of aluminosilicate and aluminate crystals and glasses. *J. Amer. Chem. Soc.* **118,** 7209–7214.

Beckett J. R. (2002) Role of basicity and tetrahedral speciation in controlling the thermodynamic properties of silicate liquids, part 1: The system $CaO-MgO-Al_2O_3-SiO_2$. *Geochim. Cosmochim. Acta* **66,** 93–107.

Behrens H. and Schulze F. (2003) Pressure dependence of melt viscosity in the system $NaAlSi_3O_8$-$CaMgSi_2O_6$. *Amer. Mineral.* **88,** 1351–1363.

Benoit M., Ispas S., and Tuckerman M. E. (2001) Structural properties of molten silicates from *ab initio* molecular-dynamics simulations: Comparison between $CaO-Al_2O_3-SiO_2$ and SiO_2. *Phys. Rev. B* **64,** 224205.

Bottinga Y. and Weill D. F. (1972) The viscosity of magmatic liquids: A model for calculation. *Am. J. Sci.* **272,** 438–475.

Bottinga Y., Richet P., and Sipp A. (1995) Viscosity regimes of homogeneous silicate melts. *Amer. Mineral.* **80,** 305–318.

Brown, G. E., Farges, F. and Calas, G. (1995) X-ray scattering and X-ray spectroscopy studies of silicate melts. In *Reviews in Mineralogy* Vol. 32 (eds. J. F. Stebbins, P. F. McMillan and D. B. Dingwell), pp. 317–410.

Daniel I., Gillet P., Poe B. T., and McMillan P. F. (1995) In-situ high-temperature Raman spectroscopic studies of aluminosilicate liquids. *Phys. Chem. Minerals* **22,** 74–86.

Daniel I., McMillan P. F., Gillet P., and Poe B. T. (1996) Raman spectroscopic study of structural changes in calcium aluminate ($CaAl_2O_4$) glass at high pressure and temperature. *Chem. Geol.* **128,** 5–15.

Dingwell D. B. (1989) Shear viscosities of ferrosilicate liquids. *Amer. Mineral.* **74,** 1038–1044.

Dingwell D. B. and Virgo D. (1987) The effect of oxidation state on the viscosity of melts in the system Na_2O-FeO-Fe_2O_3-SiO_2, *Geochim. Cosmochim. Acta.* **51,** 195–205.

Fiske P. and Stebbins J. F. (1994) The structural role of Mg in silicate liquids: A high temperature ^{25}Mg, ^{23}Na and ^{29}Si NMR study. *Amer. Mineral.* **79,** 848–861.

Hess K-U., Dingwell D. B., and Webb S. L. (1995) The influence of excess alkalis on the viscosity of a haplogranitic melt. *Amer. Mineral.* **80,** 297–304.

Kohn S. C. and Schofield P. F. (1994) The importance of melt composition in controlling trace element behaviour. *Chem. Geol.* **117,** 73–87.

Kubicki J. D. and Toplis M. J. (2002) Molecular orbital calculations on aluminosilicate tricluster molecules: Implications for the structure of aluminosilicate glasses. *Amer. Mineral.* **87,** 668–678.

Kushiro I. and Walter M. J. (1998) Mg-Fe partitioning between olivine and mafic-ultramafic melts. *Geophys. Res. Lett.* **25,** 2337–2340.

Lacy E. D. (1963) Aluminium in glasses and melts. *Phys. Chem. Glasses* **4,** 234–238.

McMillan P. F. and Kirkpatrick R. J. (1992) Al coordination in magnesium aluminosilicate glasses. *Amer. Mineral.* **77,** 898–900.

Morgan N. A. and Spera F. J. (2001) A molecular dynamics study of the glass transition in $CaAl_2Si_2O_8$: Thermodynamics and tracer diffusion. *Amer. Mineral.* **86,** 915–926.

Mysen B. O. (1988) *Structure and Properties of Silicate Melts. Developments in Geochemistry* 4, Elsevier, 354 pp.

Mysen B. O., Seifert F. A., and Virgo D. (1980) Structure and redox equilibria of iron-bearing silicate melts. *Amer. Mineral.* **65,** 867–884.

Mysen B. O., Virgo D., and Kushiro I. (1981) The structural role of aluminum in silicate melts: A Raman spectroscopic study at one atmosphere. *Amer. Mineral.* **66,** 678–701.

Mysen B. O., Virgo D., and Seifert F. A. (1984) Redox equilibria of iron in alkaline earth silicate melts: Relationships between melt structure, oxygen fugacity, temperature and properties of iron-bearing silicate liquids. *Amer. Mineral.* **69,** 834–847.

Neuville D. R (1992) Etude des propriétés thermodynamiques et rhéologiques des silicates fondus. Ph.D. thesis, Université de Paris 7–spécialité géochimie fondamentale.

Neuville D. R. and Richet P. (1991) Viscosity and mixing in molten (Ca, Mg) pyroxenes and garnets. *Geochim. Cosmochim. Acta.* **55,** 1011–1019.

Nevins D. and Spera F. J. (1998) Molecular dynamics simulations of molten $CaAl_2Si_2O_8$: Dependence of structure and properties on pressure. *Amer. Mineral.* **83,** 1220–1230.

Ohnenstetter D. and Brown W. L. (1996) Compositional variation and primary water contents of differentiated interstitial and included glasses in boninites. *Contrib. Mineral. Petrol.* **123,** 117–137.

Pickering-Witter J. and Johnston A. D. (2000) The effects of variable bulk composition on the melting systematics of fertile peridotitic assemblages. *Contrib. Mineral. Petrol.* **140,** 190–211.

Poe B. T., McMillan P. F., Coté B., Massiot D., and Coutures J. P. (1992) SiO_2-Al_2O_3 liquids: In situ study by high temperature ^{27}Al NMR spectroscopy and molecular dynamics simulations. *J. Phys. Chem.* **96,** 8220–8224.

Poe B. T., Romano C., Zotov N., Cibin G., and Marcelli A. (2001) Compression mechanisms in aluminosilicate melts: Raman and XANES spectroscopy of glasses quenched from pressures up to 10 GPa. *Chem. Geol.* **174,** 21–32.

Richet P. and Bottinga Y.(1995) Rheology and configurational entropy of silicate melts. In *Reviews in Mineralogy* **32,** 67–93. Mineralogical Society of America.

Riebling E. F. (1964) Structure of magnesium aluminosilicate liquids at 1700°C. *Can. J. Chem.* **42,** 2811–2821.

Riebling E. F. (1966) Structure of sodium aluminosilicate melts containing at least 50 mole% SiO_2 at 1500°C. *J. Chem. Phys.* **44,** 2857–2865.

Rossin R., Bersan J., and Urbain G. (1964) Etude de la viscosité de laitiers liquides appartenant au système ternaire SiO_2-Al_2O_3-CaO. *Rev. Hautes Températures et Réfractaires* **1,** 159–170.

Roy B. N. and Navrotsky A. (1984) Thermochemistry of charge-coupled substitutions in silicate glasses: The systems $M_{1/n}{}^{n+}AlO_2$-SiO_2 (M=Li, Na, K, Rb, Cs, Mg, Ca, Sr, Ba, Pb). *J. Am. Ceram. Soc.* **67,** 606–610.

Sato R. K., McMillan P. F., Dennison P., and Dupree R. (1991) A structural investigation of high alumina content glasses in the CaO-Al_2O_3-SiO_2 system via Raman and MAS NMR. *Phys. Chem. Glasses* **32,** 149–154.

Scamehorn C. and Angell C. A. (1991) Viscosity-temperature relations and structure in fully polymerised aluminosilicate melts from ion dynamics simulations. *Geochim. Cosmochim. Acta* **55,** 721–730.

Schwab B. and Johnston A. D. (2001) Melting systematics of modally variable, compositionally intermediate peridotites and the effects of mineral fertility. *J. Petrol.* **42,** 1789–1811.

Shibata Y., Takahashi E., and Matsuda J. (1998) Solubility of neon, argon, krypton and xenon in binary and ternary silicate systems: A new view on noble gas solubility. *Geochim. Cosmochim. Acta* **62,** 1241–1253.

Solvang M., Yue Y. Z., Jensen S. L., and Dingwell D. B. (2004) Rheological and thermodynamic behaviors of different calcium aluminosilicate melts with the same non-bridging oxygen content. *J. Non-Cryst. Solids* **336,** 179–188.

Stebbins J. F. (1991) Experimental confirmation of five-coordinated silicon in a silicate glass at 1 atmosphere pressure. *Nature* **351,** 638–639.

Stebbins J. F. (1995) Dynamics and structure of silicate and oxide melts: Nuclear magnetic resonance studies. *Rev. Mineral.* **32,** 191–246.

Stebbins J. F., Kroeker S., Lee S. K., and Kiczenski T. J. (2000) Quantification of five- and six-coordinated aluminum in aluminosilicate and fluoride-containing glasses by high-field, high-resolution ^{27}Al NMR. *J. Non-Cryst. Solids* **275,** 1–6.

Stebbins J. F., Oglesby J. V., and Kroeker S. (2001) Oxygen triclusters in crystalline $CaAl_4O_7$ (grossite) and in calcium aluminosilicate glasses: O-17 NMR. *Amer. Mineral.* **86,** 1307–1311.

Stebbins J. F. and Xu Z. (1997) NMR evidence for excess non-bridging oxygen in an aluminosilicate glass. *Nature* **390,** 60–62.

Tauber P. and Arndt J. (1987) The relationship between viscosity and temperature in the system anorthite-diopside. *Chem. Geol.* **62,** 71–81.

Taylor M. and Brown G. E. (1979a) Structure of mineral glasses — I The feldspar glasses $NaAlSi_3O_8$, $KAlSi_3O_8$, $CaAl_2Si_2O_8$. *Geochim. Cosmochim. Acta* **43,** 61–77.

Taylor M. and Brown G. E. (1979b) Structure of mineral glasses — II The SiO_2-$NaAlSiO_4$ join. *Geochim. Cosmochim. Acta* **43,** 1467–1475.

Tinker D., Lesher C. E., and Hutcheon I. D. (2003) Self-diffusion of Si and O in diopside-anorthite melt at high pressures. *Geochim. Cosmochim. Acta* **67,** 133–142.

Toplis M. J. (1998) Energy barriers to viscous flow and the prediction of glass transition temperatures of molten silicates. *Amer. Mineral.* **83,** 480–490.

Toplis M. J. and Dingwell D. B. (1996) The variable influence of P_2O_5 on the viscosity of melts of differing alkali/aluminium ratio: Implications for the structural role of phosphorus in silicate melts. *Geochim. Cosmochim. Acta* **60,** 4107–4121.

Toplis M. J. and Corgne A. (2002) An experimental study of element partitioning between magnetite, clinopyroxene and iron-bearing silicate liquids with particular emphasis on vanadium. *Contrib. Mineral. Petrol.* **144,** 22–37.

Toplis M. J. and Schaller T. (1998) A ^{31}P MAS NMR study of glasses in the system $x$$Na_2O$-(1-$x$)$Al_2O_3-2SiO_2$-$y$$P_2O_5$. *J. Non-Cryst. Solids* **224,** 57–68.

Toplis M. J., Dingwell D. B., and Lenci T. (1997) Peraluminous viscosity maxima in Na_2O-Al_2O_3-SiO_2 liquids: The role of triclusters in tectosilicate melts. *Geochim. Cosmochim. Acta* **61,** 2605–2612.

Toplis M. J., Kohn S. C., Smith M. E., and Poplett I. J. F. (2000) Fivefold-coordinated aluminum in tectosilicate glasses observed by triple quantum MAS NMR. *Amer. Mineral.* **85,** 1556–1560.

Urbain G., Bottinga Y., and Richet P. (1982) Viscosity of liquid silica, silicates and aluminosilicates. *Geochim. Cosmochim. Acta* **46,** 1061–1071.

Walter M. J. (1998) Melting of garnet peridotite and the origin of komatiite and depleted lithosphere. *J. Petrol.* **39,** 29–60.

Wiedenroth A., and Rüssel R. (2003) Voltammetric studies in iron-doped $5Na_2O \cdot xMgO \cdot (15\text{-}x)CaO \cdot yAl_2O_3 \cdot (80\text{-}y)SiO_2$ melts. *J. Non-Cryst. Solids* **318,** 79–86.

Yarger J. L., Smith K. H., Nieman R. A., Diefenbacher J., Wolf G. H., Poe B. T., and McMillan P. F. (1995) Al coordination changes in high pressure aluminosilicate liquids. *Science* **270,** 1964–1967.